Next, to further investigate micelle destabilization due to disulfide reduction as well as the stabilizing effect of Chol moieties, agarose gel electrophoresis of micelle samples was performed after incubation with or without DTT in the presence of varying concentrations of dextran sulfate (MW = 5000). This strong polyanion was used for mimicking the negatively charged extracellular matrixes, as a recent study reported that those polyanionic components play a crucial role for the destabilization of blood circulating siRNA PICs [36]. The stabilizing effect of Chol moiety was again observed upon analysis of siRNA release induced by the counter polyanions. Chol-siRNA micelles required larger amounts of dextran sulfate for the appearance of the released siRNA band, compared to Chol-free micelles (Fig. 3B and C). Futhermore, the decreased stability under the reductive conditions was confirmed for Chol-siRNA micelles, as the incubation under 100 mM DTT apparently decreased the amount of dextran sulfate required to release free siRNA from micelles (Fig. 3B and C). The similar facilitated siRNA release profiles were also observed for Chol-siRNA micelles under a cytoplasm-mimicking condition (10 mM DTT and 150 mM NaCl) in comparison with a cell exterior-mimicking condition (10 μM DTT and 150 mM NaCl) (Fig. S5A and B). Nevertheless, the modest difference between non-reductive and reductive conditions implies the significant, yet restricted contribution of disulfide cross-linking to the resistance of micelles against a strong polyanion. Note that the stabilizing effect of disulfide cross-linking was more evident under milder conditions where micelle samples were incubated with an anionic lipid molecule (DOPS). In this experiment, micelle sensitivity to reductive conditions was clearly observed even for Chol-free micelles (Fig. S5C and D).

3.4. In vitro efficacy of actively-targeted/stabilized micelles

To verify the biological effect of cRGD ligand as well as the stabilizing effect of Chol-siRNA, cellular uptake efficiencies of siRNA micelle formulations were compared by flow cytometric analyses. In this experiment, the fluorescence intensity of HeLa-Luc cells was determined after their treatment with micelles prepared with Cy5-siRNA. Note that HeLa-Luc cells were chosen as a target cell line because they overexpress integrins, especially $\alpha_v\beta_5$, on their cellular surface (Fig. S6) [31,37], and are thus appropriate for assessing the cRGD effect on cellular uptake of siRNA. Significantly higher fluorescence intensity was observed for cRGD-installed micelles, i.e., RGD(+)/Chol(−) and RGD(+)/Chol(+) micelles, in comparison with control micelles without cRGD, i.e., RGD(−)/Chol(−) and RGD(−)/Chol(+) micelles (Fig. 4A). These results highlight the effect of cRGD on the enhanced cellular uptake of siRNA micelles. In the absence of cRGD ligand, the cells incubated with RGD(−)/Chol(+) micelles showed modestly higher fluorescence intensity than those incubated with RGD(−)/Chol(−) micelles, indicating that Chol-siRNA facilitated the cellular uptake of RGD(−) micelles. Apparently, the Chol-siRNA was more effective for improving the cellular uptake of non-targeted RGD(−) micelles, compared to the targeted RGD(+) micelles. These different effects of Chol-siRNA can be explained from the standpoint of cellular uptake rate of micelles; the targeted RGD(+) micelles may be internalized more rapidly and less affected by micelle stability in cell culture conditions, compared to the non-targeted RGD(−) micelles.

Next, *in vitro* gene silencing ability of the actively-targeted/stabilized (RGD(+)/Chol(+)) micelles was evaluated by comparing with those of the other micelle formulations. siRNA for luciferase gene, i.e., siLuc, was selected for this luminescence-based gene silencing assay, which allows quantitative determination of gene silencing by comparing the luminescence intensity among samples. Fig. 4B shows the relative luminescence intensity of cells treated with each siRNA micelle (or naked siRNA) at 200 nM siRNA after 50 h incubation. The observed *in vitro* gene silencing activity is in good agreement with the results from the cellular uptake study (Fig. 4A); as cRGD-installed, RGD(+)/Chol(+) and RGD(+)/Chol(−) micelles achieved the most efficient luciferase gene silencing, followed by the RGD(−)/Chol(+) micelles and the RGD(−)/Chol(−) micelles. Actively-targeted micelles prepared with siScr induced no significant decrease in relative luminescence intensity, confirming the sequence-specific gene silencing activity of actively-targeted micelles. Consequently, the cRGD ligands installed on the micelle surface enhanced *in vitro* gene silencing activity of siRNA micelles regardless of the Chol moiety conjugated to siRNA. This is consistent with the result seen in Fig. 3A; the Chol-free micelles could avoid the rapid dissociation in the 10% serum-containing PBS under 200 nM siRNA corresponding to the transfection condition, presumably enabling ligand-mediated rapid cellular uptake. It should be noted in this regard that the Chol-free siRNA micelles prepared with cRGD-PEG-PLL without thiol (or other stabilizing) moieties induced no gene silencing under similar conditions as we reported previously [13], indicating the impact of disulfide cross-linking on gene silencing efficiency.

Cell viability following treatment with siRNA micelles was also examined in order to exclude the possibility of cytotoxic effects on the gene silencing activity of siRNA micelles. RGD(+)/Chol(−) micelles and RGD(+)/Chol(+) micelles, which showed the highest gene silencing activity, were subjected to a cell viability assay using the commercially available CCK-8 kit, based on a water soluble tetrazolium salt (WST-8). Neither micelle formulation induced significant cytotoxicity even at a high concentration of siRNA (1000 nM) (Fig. S7), indicating negligible cytotoxic effects of siRNA micelles at concentrations used for the gene silencing studies. Considering that homopolymer PLLs with a high molecular weight (e.g. 27 kDa) are known to induce significant cytotoxicity due to their cationic charges [38], this negligible cytotoxicity of the siRNA micelles might be the result that they were composed of a relatively shorter PLL segment and equipped with a PEG outer layer that masked the charged component.

3.5. In vivo efficacy of actively-targeted/stabilized micelles

Since enhanced micelle stability and active targeting ability were both demonstrated under *in vitro* conditions (Figs. 3 and 4A and B), the *in vivo* behaviors of actively-targeted/stabilized micelles were investigated following systemic administration. The longevity of siRNA micelles in the bloodstream is a critical factor for tumor accumulation of macromolecules. Prolonged circulation results in increased contact opportunity for actively-targeted micelles with the cellular surface receptors in tumor tissues.

First, the blood circulation property of fluorescently-labeled micelles (prepared with Cy5-siRNA) was evaluated by IVRT-CLSM, which can continuously monitor the fluorescence intensity of Cy5-siRNA (or its micelles) circulating in the blood of mice immediately after intravenous injection (Fig. S8A). Fluorescence intensities determined from ROIs selected within the vein were plotted against time to compare blood retention profiles of different micelle formulations (Fig. 5A). In this regard, non-targeted micelles were utilized for simply validating the effect of Chol-siRNA encapsulated within the micelles on blood retention. Chol-free micelles were rapidly eliminated from circulation, similar to naked siRNA, and consequently their blood half-life ($T_{1/2}$) was within 5 min. In sharp contrast, Chol-siRNA micelles showed significantly longer blood retention time ($T_{1/2}$ = >20 min, $p < 0.05$) than Chol-free micelles. This prolonged blood circulation observed for Chol-siRNA micelles is in good agreement with the results demonstrating higher stability against dilution with serum-containing PBS (Fig. 3A) and improved resistance to polyanion

exchange with polysulfates (Fig. 3C). It is also worth mentioning that the elimination of Chol-siRNA micelles from the bloodstream followed a single exponential decay (or a one-compartment model in pharmacokinetics) (Fig. S8B), suggesting that the Chol-siRNA micelles were eliminated mainly from the kidney without being distributed into peripheral tissues. This is supported by the result that the Chol-siRNA micelles (or the siRNA payloads) were mainly accumulated in the kidney after systemic administration (Fig. S9). Note that the blood retention time of naked Chol-siRNA was modestly longer than those of naked Chol-free siRNA. This may be due to interaction of Chol-siRNA with lipoproteins in the bloodstream leading to compromised renal filtration [39].

Next, the tumor-targeting ability of cRGD-installed micelles was investigated by measuring their accumulation in subcutaneous HeLa-Luc tumors. Fluorescently-labeled micelles were administered by tail vein injection and tumors were excised after 4 h followed by measurement of the fluorescence intensity of each tumor mass with an IVIS instrument. While there was almost no difference in fluorescence intensity between Chol-free micelles with and without cRGD, significantly higher fluorescence intensity was observed for Chol-siRNA micelles equipped with cRGD, compared to those without cRGD (Fig. 5B). These results indicate that the cRGD ligand enabled more efficient tumor accumulation of the highly stabilized Chol-siRNA micelles following systemic administration, presumably due to the enhanced avidity of cRGD ligands to $\alpha_v\beta_3/\alpha_v\beta_5$ integrin receptors on cancerous cells and also tumor-associated endothelial cells [13,33,34]. Intratumoral distribution of RGD(+)/Chol(+) micelles was further examined by continuous CLSM observation of the subcutaneous tumor tissue after systemic administration. The CLSM image captured at 80 min after injection displays massive distribution of the micelles in the tumor tissue through the blood vessels (Fig. S10). Importantly, there were no significant differences in healthy organ/tissue accumulation between non-targeted and actively-targeted micelles ($p > 0.05$) (Fig. S9), demonstrating tumor-selective targeting of RGD(+)/Chol(+) micelles.

Finally, the *in vivo* gene silencing activity of siRNA micelles was investigated through luciferase gene silencing (luminescence measurement) in subcutaneous HeLa-Luc tumors, similar to the luminescence-based assay used for *in vitro* experiments. At 48 h after the initial injection of samples (total 3 intravenous injections), luciferin solution was intraperitoneally injected into mice, followed by measurement of the luminescence intensity in the tumor tissues with an IVIS instrument (Fig. 5C and Fig. S11). Non-targeted RGD(−)/Chol(−) micelles did not decrease tumor luminescence intensity, whereas the actively-targeted, RGD(+)/Chol(−) and RGD(+)/Chol(+) micelles did reduce tumor luminescence intensities compared to buffer-treated controls. In particular, the actively-targeted/stabilized, RGD(+)/Chol(+) micelles achieved significant decrease in the luminescence intensity ($p < 0.05$ for buffer-treated controls). It should be noted that the RGD(+)/Chol(+) micelles carrying siScr as a control sequence caused no decrease in the luminescence intensity, demonstrating sequence-specific gene silencing (i.e. RNAi) activity of the actively-targeted/stabilized micelles. In addition, it was also confirmed that all the tested micelles did not induce significant changes in the body weight of tumor-bearing mice (Table S1). In total, actively-targeted and stabilized micelles were more effective in delivering intact (thus active) siRNA to the cytoplasm of tumor cells following systemic administration. The present study particularly focused on the separate functionalization of the macromolecular components, i.e., PEG-PLL and siRNA, for construction of the multifunctional formulation, i.e., actively-targeted/stabilized micelles. This approach permitted the facile functionalization based on a simple chemistry, which is in contrast to the previously developed block copolymer modified with 2-iminothiolane, where two functional groups, open chain and closed ring structures, are equilibrated in the side chain of PLL [13].

4. Conclusions

Actively-targeted and stabilized PIC micelles were constructed with Chol-siRNA and PEG-PLL comprising the cRGD ligand at the PEG terminus and thiol (and amidine) functionality in PLL side chains, for systemic siRNA delivery to solid tumors. The Chol modification of siRNA allowed the production of PIC micelles at wider mixing ratios above the charge-stoichiometric point and dramatically stabilized the micelle structure, resulting in the enhanced blood circulation property of siRNA micelles. Further, the active targeting ability of the cRGD ligand was proven by enhanced cellular uptake *in vitro* and also enhanced tumor accumulation *in vivo* following systemic administration. Ultimately, the synergistic effect of active targetability and improved stability enabled significant sequence-specific gene silencing in the subcutaneous tumor tissue following systemic administration of siRNA micelles. The results obtained in this study highlight the importance of additional stabilizing mechanisms in PIC micelle systems, and that stabilization can be achieved from both the polymer component and the siRNA component used. Here, Chol-conjugation to siRNA reinforced the limited effect of disulfide cross-linking, thus improving the active targetability of nanoparticulate formulations for systemic transport of siRNA into tumor tissues.

Acknowledgments

This research was financially supported by the Funding Program for World-Leading Innovate R&D in Science and Technology (FIRST) (JSPS), Grants-in-Aid for Scientific Research of MEXT (JSPS KAKENHI Grant Numbers 25000006 and 25282141), the Center of Innovation (COI) Program (JST), Grants-in-Aid for Scientific Research of MHLW, National Institute of Biomedical Innovation and Mochida Memorial Foundation for Medical and Pharmaceutical Research.

Appendix A. Supplementary data

Supplementary data related to this article can be found online at http://dx.doi.org/10.1016/j.biomaterials.2014.05.041.

References

[1] Fire A, Xu S, Montogomery M, Kostas S, Driver S, Mello C. Potent and specific genetic interference by double stranded RNA in caenorhabditis elegans. Nature 1998;391:806–11.
[2] Elbashir SM, Harborth J, Lendeckel W, Yalcin A, Weber K, Tuschl T. Duplexes of 21-nucleotide RNAs mediate RNA interference in cultured mammalian cells. Nature 2001;411:494–8.
[3] Burnett JC, Rossi JJ. RNA-based therapeutics: current progress and future prospects. Chem Biol Rev 2012;19:60–71.
[4] Carthew R, Sontheimer E. Origins and mechanisms of miRNA and siRNAs. Cell 2009;136:642–55.
[5] Turner J, Jones S, Moschos S, Lindsay M, Gait M. MALDI-TOF mass spectral analysis of siRNA degradation in serum confirms an RNase A-like activity. Mol Biosyst 2007;3:43–50.
[6] Van de Water F, Boerman O, Wouterse A, Peters J, Russel F, Masereeuw R. Intravenously administered short interfering RNA accumulates in the kidney and selectively suppresses gene function in renal proximal tubules. Drug Metab Dispos 2006;34:1393–7.
[7] Schiffelers RM, Ansari A, Xu J, Zhou Q, Tang Q, Strom G, et al. Cancer siRNA therapy by tumor selective delivery with ligand-targeted sterically stabilized nanoparticle. Nucleic Acids Res 2004;32:e149.
[8] Song E, Zhu P, Lee SK, Chowdhury D, Kussman S, Dykxhoorn DM, et al. Antibody mediated in vivo delivery of small interfering RNAs via cell-surface receptors. Nat Biotechnol 2005;23:709–17.

[9] McNamara II JO, Andrechek ER, Wang Y, Viles KD, Rempel RE, Gilboa E, et al. Cell type-specific delivery of siRNAs with aptamer-siRNA chimeras. Nat Biotechnol 2006;24:1005–15.
[10] Li SD, Chen YC, Hackett MJ, Huang L. Tumor-targeted delivery of siRNA by self-assembled nanoparticles. Mol Ther 2008;16:163–9.
[11] Wang XL, Xu R, Wu X, Gillespie D, Jensen R, Lu ZR. Targeted systemic delivery of a therapeutic siRNA with a multifunctional carrier controls tumor proliferation in mice. Mol Pharm 2009;6:738–46.
[12] Davis ME, Zuckerman JE, Choi CHJ, Seligson D, Tolcher A, Alabi CA, et al. Evidence of RNAi in humans from systemically administered siRNA via targeted nanoparticles. Nature 2010;64:1067–70.
[13] Christie RJ, Matsumoto Y, Miyata K, Nomoto T, Fukushima S, Osada K, et al. Targeted polymeric micelles for siRNA treatment of experimental cancer by intravenous injection. ACS Nano 2012;6:5174–89.
[14] Dohmen C, Edinger D, Frohlich T, Schreiner L, Lachelt U, Troiber C, et al. Nanosized multifunctional polyplexes for receptor-mediated siRNA delivery. ACS Nano 2012;26:5198–208.
[15] Lee H, Lytton-Jean AKR, Chen Y, Love KT, Park AI, Karagiannis ED, et al. Molecularly self-assembled nucleic acid nanoparticles for targeted in vivo siRNA delivery. Nat Nanotechnol 2012;7:389–93.
[16] Kim HJ, Ishii T, Zheng M, Watanabe S, Toh K, Matsumoto Y, et al. Multifunctional polyion complex micelle featuring enhanced stability, targetability, and endosome escapability for systemic siRNA delivery to subcutaneous model of lung cancer. Drug Deliv Transl Res 2014;4:50–60.
[17] Jule E, Nagasaki Y, Kataoka K. Surface plasmon resonance study on the interaction between lactose-installed poly(ethylene glycol)-poly(D, L-lactide) block copolymer micelles and lectins immobilized on a gold surface. Langmuir 2002;18:10334–9.
[18] Alam MR, Ming X, Fisher M, Lackey JG, Rajeev KG, Manoharan M, et al. Multivalent cyclic RGD conjugates for targeted delivery of small interfering RNA. Bioconjug Chem 2011;22:1673–81.
[19] Harada A, Kataoka K. Formation of polyion complex micelles in an aqueous milieu from a pair of oppositely-charged block copolymers with poly(ethylene glycol) segments. Macromolecules 1995;28:5294–9.
[20] Kataoka K, Togawa H, Harada A, Yasugi K, Matsumoto T, Katayose S. Spontaneous formation of polyion complex micelles with narrow distribution from antisense oligonucleotide and cationic block copolymer in physiological saline. Macromolecules 1996;29:8556–7.
[21] Kakizawa Y, Kataoka K. Block copolymer micelles for delivery of gene and related compounds. Adv Drug Deliv Rev 2002;54:203–22.
[22] Miyata K, Nishiyama N, Kataoka K. Rational design of smart supramolecular assemblies for gene delivery: chemical challenges in the creation of artificial viruses. Chem Soc Rev 2012;41:2562–74.
[23] Kim HJ, Oba M, Pittella F, Nomoto T, Cabral H, Matsumoto Y, et al. PEG-detachable cationic polyaspartamide derivatives bearing stearoyl moieties for systemic siRNA delivery toward subcutaneous BxPC3 pancreatic tumor. J Drug Target 2012;20:33–42.
[24] Kakizawa Y, Harada A, Kataoka K. Environment-sensitive stabilization of core-shell structured polyion complex micelle by reversible cross-linking of the core through disulfide bond. J Am Chem Soc 1999;121:11247–8.
[25] Matsumoto S, Christie RJ, Nishiyama N, Miyata K, Ishii A, Oba M, et al. Environment-responsive block copolymer micelles with a disulfide cross-linked core for enhanced siRNA delivery. Biomacromolecules 2009;10:119–27.
[26] Christie RJ, Miyata K, Matsumoto Y, Nomoto T, Menasco D, Lai TC, et al. Effect of polymer structure on micelles formed between siRNA and cationic block copolymer comprising thiols and amidines. Biomacromolecules 2011;12:3174–85.
[27] Meister A, Anderson ME. Glutathione. Annu Rev Biochem 1983;52:711–60.
[28] Saito G, Swanson JA, Lee KD. Drug delivery strategy utilizing conjugation via reversible disulfide linkages: role and site of cellular reducing activities. Adv Drug Deliv Rev 2013;55:199–215.
[29] Soutschek J, Akinc A, Bramlage B, Charisse K, Constien R, Donoghue M, et al. Therapeutic silencing of an endogenous gene by systemic administration of modified siRNAs. Nature 2004;432:173–8.
[30] Oba M, Miyata K, Osada K, Christie RJ, Sanjoh M, Li W, et al. Polyplex micelles prepared from ω-cholesteryl PEG-polycation block copolymers for systemic gene delivery. Biomaterials 2011;32:652–63.
[31] Oba M, Fukushima S, Kanayama N, Aoyagi K, Nishiyama N, Koyama H, et al. Cyclic RGD peptide-conjugated polyplex micelles as a targetable gene delivery system directed to cells possessing αvβ3 and αvβ5 integrins. Bioconjug Chem 2007;18:1415–23.
[32] Matsumoto Y, Nomoto T, Cabral H, Mastumoto Y, Watanabe S, Christie RJ, et al. Direct and instantaneous observation of intravenously injected substances using intravital confocal micro-videography. Biomed Opt Express 2010;1:1209–16.
[33] Ruoslahti E. RGD and recognition sequences for integrins. Annu Rev Cell Dev Biol 1996;12:697–715.
[34] Xiong J, Stehle T, Zhang R, Joachimiak A, Frech M, Goodman S, et al. Crystal structure of the extra-cellular segment of integrin αvβ3 in complex with an Arg-Gly-Asp ligand. Science 2002;296:151–5.
[35] Itaka K, Yamauchi K, Harada A, Nakamura K, Kawaguchi H, Kataoka K. Polyion complex micelles from plasmid DNA and poly(ethyleneglycol)-poly(L-lysine) block copolymer as serum-tolerable polyplex system: physicochemical properties of micelles relevant to gene transfection efficiency. Biomaterials 2003;24:4495–506.
[36] Zukerman JE, Choi CHJ, Han H, Davis ME. Polycation-siRNA nanoparticles can disassemble at the kidney glomerular basement membrane. Proc Natl Acad Sci U S A 2012;109:3137–42.
[37] Shayakhmetov DM, Eberly AM, Li ZY, Lieber A. Deletion of penton RGD motifs affects the efficiency of both the internalization and the endosome escape of viral particles containing adenovirus serotype 5 or 35 fiber knobs. J Virol 2005;79:1053–61.
[38] Symonds P, Murray JC, Hunter AC, Debska G, Szewczyk A, Moghimi SM. Low and high molecular weight poly(L-lysine)s/poly(L-lysine)-DNA complexes initiate mitochondrial-mediated apoptosis differently. FEBS Lett 2005;579:6191–8.
[39] Wolfrum C, Shi S, Jayaprakash KN, Jayaraman M, Wang G, Pandey RK, et al. Mechanisms and optimization of *in vivo* delivery of lipophilic siRNAs. Nat Biotechnol 2007;25:1149–57.

Journal of Controlled Release 178 (2014) 18–24

Contents lists available at ScienceDirect

Journal of Controlled Release

journal homepage: www.elsevier.com/locate/jconrel

Systemic siRNA delivery to a spontaneous pancreatic tumor model in transgenic mice by PEGylated calcium phosphate hybrid micelles

Frederico Pittella [a,b], Horacio Cabral [b], Yoshinori Maeda [b], Peng Mi [c], Sumiyo Watanabe [a], Hiroyasu Takemoto [c], Hyun Jin Kim [d], Nobuhiro Nishiyama [c], Kanjiro Miyata [a,*], Kazunori Kataoka [a,b,d,e,**]

[a] Center for Disease Biology and Integrative Medicine, Graduate School of Medicine, The University of Tokyo, 7-3-1 Hongo, Bunkyo-ku, Tokyo 113-0033, Japan
[b] Department of Bioengineering, Graduate School of Engineering, The University of Tokyo, 7-3-1 Hongo, Bunkyo-ku, Tokyo 113-8656, Japan
[c] Polymer Chemistry Division, Chemical Resources Laboratory, Tokyo Institute of Technology, R1-11, 4259 Nagatsuta, Midori-ku, Yokohama 226-8503, Japan
[d] Department of Materials Engineering, Graduate School of Engineering, The University of Tokyo, 7-3-1 Hongo, Bunkyo-ku, Tokyo 113-8656, Japan
[e] Center for NanoBio Integration, The University of Tokyo, 7-3-1 Hongo, Bunkyo-ku, Tokyo 113-8656, Japan

ARTICLE INFO

Article history:
Received 3 August 2013
Accepted 7 January 2014
Available online 15 January 2014

Keywords:
siRNA delivery
Calcium phosphate
PEG
Charge-conversional polymer
Transgenic mice
Spontaneous pancreatic carcinoma

ABSTRACT

Efficient systems for delivery of small interfering RNA (siRNA) are required for clinical application of RNA interference (RNAi) in cancer therapy. Herein, we developed a safe and efficient nanocarrier comprising poly(ethylene glycol)-*block*-charge-conversional polymer (PEG-CCP)/calcium phosphate (CaP) hybrid micelles for systemic delivery of siRNA and studied their efficacy in spontaneous bioluminescent pancreatic tumors from transgenic mice. PEG-CCP was engineered to provide the siRNA-loaded hybrid micelles with enhanced colloidal stability and biocompatibility due to the PEG capsule and with endosome-disrupting functionality due to the acidic pH-responsive CCP segment where the polyanionic structure could be converted to polycationic structure at acidic pH through *cis*-aconitic amide cleavage. The resulting hybrid micelles were confirmed to have a diameter of <50 nm, with a narrow size distribution. Intravenously injected hybrid micelles significantly reduced the luciferase-based luminescent signal from the spontaneous pancreatic tumors in an siRNA sequence-specific manner. The gene silencing activity of the hybrid micelles correlated with their preferential tumor accumulation, as indicated by fluorescence imaging and histological analysis. Moreover, there were no significant changes in hematological parameters in mice treated with the hybrid micelles. These results demonstrate the great potential of the hybrid micelles as siRNA carriers for RNAi-based cancer therapy.

1. Introduction

Small interfering ribonucleic acid (siRNA) provides new perspectives for the treatment of various diseases. It functions by obstructing a specific cellular process by reducing protein production in a sequence-specific manner, a phenomenon termed RNA interference (RNAi) [1–4]. In particular, the use of RNAi-based therapy is expected to have potential for treatment of cancer because cancerous cells overexpress several specific genes, including oncogenes [5,6]. In the development of an RNAi-based cancer therapy, systemic administration of siRNA is essential for its effective accumulation in the wide range of internal tumor tissues. However, intravenous injection of naked siRNA molecules results in their rapid enzymatic degradation and subsequent clearance through the kidneys [7,8]. Therefore, efficient carriers are required to ensure successful delivery of siRNA to the therapeutic site of action [3,6,9].

Calcium phosphate (CaP)-based nanocarriers, a promising delivery system, has been widely developed for delivering nucleic acids to mammalian cells [10–14]. These are readily prepared by mixing aqueous ionic solutions for efficient encapsulation of nucleic acids. In this regard, we have previously prepared poly(ethylene glycol) (PEG)-coated CaP hybrid micelles by utilizing PEG-polyanion block copolymers [12,15–20]. In these block copolymers, the polyanion segment acts as a binding moiety with CaP nanoparticles, whereas the PEG segment forms a nonionic and hydrophilic outer layer for enhanced colloidal stability and biocompatibility (Fig. 1A). Furthermore, our recent studies successfully demonstrated functionalization of the polyanion segment for efficient endosomal escape of the siRNA payload [19–21]. An acidic pH-responsive anionic moiety, *cis*-aconitic amide (Aco), was introduced into the cationic side chain of the endosome-disrupting polyaspartamide derivative, poly{*N*′-[*N*-(2-aminoethyl)-2-aminoethyl] aspartamide} (PAsp(DET)) (Fig. 1B). The obtained PAsp(DET-Aco) bearing a net negative charge was found to be inactive for membrane disruption at extracellular neutral pH. However, on reversion to the parent polycation PAsp(DET) by cleavage of the Aco moiety at endosomal acidic pH, membrane disruptivity was activated [thus, termed charge-conversional polymer (CCP)] (Fig. 1C) [22]. Ultimately, the systemic administration of PEG-CCP/CaP hybrid micelles carrying

* Corresponding author. Tel.: +81 3 5841 1701; fax: +81 3 5841 7139.
** Correspondence to: K. Kataoka, Center for Disease Biology and Integrative Medicine, Graduate School of Medicine, The University of Tokyo, 7-3-1 Hongo, Bunkyo-ku, Tokyo 113-0033, Japan. Tel.: +81 3 5841 7138; fax: +81 3 5841 7139.
E-mail addresses: miyata@bmw.t.u-tokyo.ac.jp (K. Miyata), kataoka@bmw.t.u-tokyo.ac.jp (K. Kataoka).

0168-3659/$ – see front matter © 2014 Elsevier B.V. All rights reserved.
http://dx.doi.org/10.1016/j.jconrel.2014.01.008

vascular endothelial growth factor (VEGF) siRNA achieved significant antitumor activity in a murine xenograft model of subcutaneous pancreatic tumors [20]. These results demonstrated the great potential of this system for use as a cancer therapy and motivated us to investigate this system further.

To confirm the translational capability of promising nanocarriers, relevant preclinical tumor models, which parallel the microenvironment characteristics of tumors in the clinic, should be considered. In animal tumor models prepared by implantation of exogenous cancer cells or tissues, the tumoral microenvironment presents substantial differences with that of tumors in patients, including stroma, vasculature, lymphatics, immune cells, and increased population of certain clonal fractions due to selective stresses during cell culture or tissue transplantation [23,24]. These features in transplanted models are expected to affect the nanocarrier-mediated delivery of siRNA as well as drugs, *e.g.*, efficiencies of penetration, accumulation, and gene silencing in tumor tissues. In this regard, in genetically engineered tumor models, the tumor development closely relates to the clinical setting of the disease, with immune responses, angiogenesis, and inflammation naturally interrelating with the tumor [23]. Therefore, by using such spontaneous tumor models, siRNA-loaded nanocarriers could be evaluated in tumors with more relevant microenvironment and cell populations.

In the present study, we applied siRNA-loaded hybrid micelles in a genetically engineered pancreatic tumor model, in which the tumor gradually arises *in situ* and is associated with normal immune, angiogenesis, and inflammatory processes. The EL1-Luc/TAg transgenic mice used in this study spontaneously develop bioluminescent pancreatic adenocarcinoma owing to the SV40 T and firefly luciferase transgene constructs, which are regulated by the rat EL1 promoter [25]. SV40 T alters molecular, physiological, and histological aspects comparable to the tumorigenesis of acinar cell carcinoma in humans. Moreover, EL1-Luc/TAg transgenic mice permit non-invasive tracing of tumors through bioluminescence imaging because the cancer cells exclusively express luciferase. Accordingly, *in vivo* RNAi activity of the hybrid micelles carrying luciferase siRNA (siLuc) was determined by quantifying the luminescent signal from the pancreatic tumors after intravenous injection. To verify the validity of the measured RNAi activity, the tumor accumulation profile of the hybrid micelles was further assessed. To the best of our knowledge, this is the first study to demonstrate the effective delivery of siRNA to a spontaneous tumor model in transgenic mice by systemic administration.

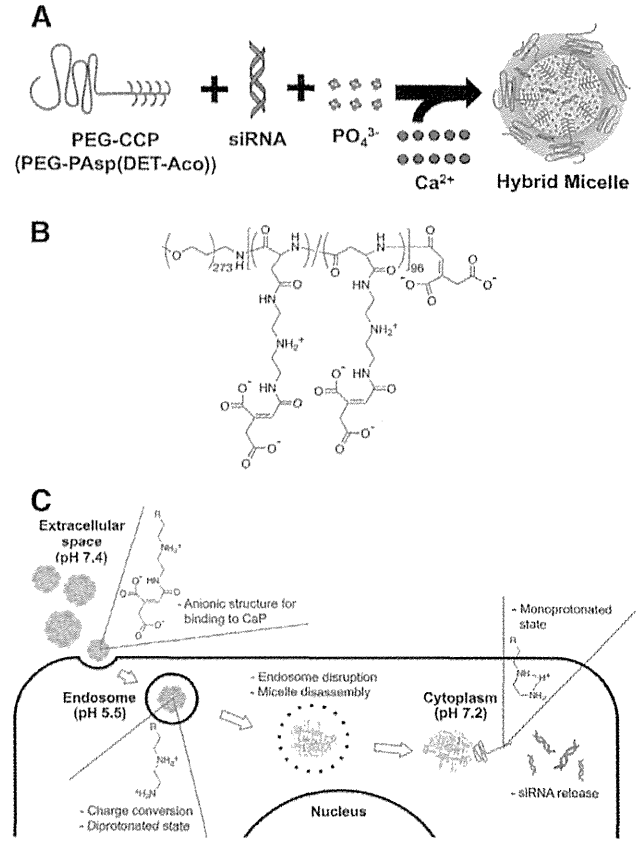

Fig. 1. (A) Schematic illustration of the preparation of hybrid micelles with PEG-CCP, siRNA, and CaP. (B) Chemical structure of PEG-PAsp(DET-Aco), termed PEG-CCP. (C) Schematic illustration of the cellular delivery of siRNA by PEG-CCP/CaP hybrid micelles. At extracellular neutral pH, PEG-CCP binds to the CaP nanoparticle, generating a PEG outer layer. Once endocytosed by the cell, the hybrid micelles undergo endosomal acidification. During acidification, PEG-CCP is converted to the parent PEG-PAsp(DET) through cleavage of the *cis*-aconitic amide bond, exposing the diprotonated side chain structure for endosomal membrane disruption. Finally, the siRNA payload is released into the cytoplasm, while the PAsp(DET) segment adopts the membrane-inactive monoprotonated side chain at cytoplasmic neutral pH.

2. Materials and methods

2.1. Materials, cell lines, and animals

$CaCl_2$ (anhydrous), Na_3PO_4, NaCl, HCl, ethanol, and phosphate buffered saline (PBS) were purchased from Wako Pure Chemical Industries Ltd. (Osaka, Japan). Dulbecco's modified Eagle's medium (DMEM) and penicillin/streptomycin stabilized solution were purchased from Sigma-Aldrich (St. Louis, MO). *In vivo* grade luciferin VivoGlo, cell culture lysis buffer, and the Luciferase Assay System were purchased from Promega Corporation (Madison, WI). Tissue-Tek OCT compound and fetal bovine serum (FBS) were acquired from Sakura Finetek USA, Inc. (Torrance, CA) and Dainippon Sumitomo Pharma Co., Ltd. (Osaka, Japan), respectively. Methoxy-poly(ethylene glycol)-*block*-poly(*N*″-{*N*′-[(*N*-*cis*-aconityl)-2-aminoethyl]-2-aminoethyl}aspartamide) (PEG-PAsp(DET-Aco) or PEG-CCP) was synthesized as previously described, and then characterized by ^{1}H NMR (PEG: 12 kDa; PAsp(DET-Aco): 34 kDa) [19,20]. Firefly luciferase siRNA (siLuc) and its control siRNA (siScr) were synthesized by Hokkaido System Science (Hokkaido, Japan). The sequences of the siLuc were: 5′-CUU ACG CUG AGU ACU UCG AdTdT-3′ (sense) and 5′-UCG AAG UAC UCA GCG UAA GdTdT-3′ (antisense); the sequences of the siScr were: 5′-UUC UCC GAA CGU GUC ACG UdTdT-3′ (sense) and 5′-ACG UGA CAC GUU CGG AGA AdTdT-3′ (antisense). Fluorescently labeled siLuc was obtained by introducing Alexa Fluor 647 to the 5′ end of sense strand from GeneDesign, Inc. (Osaka, Japan).

HeLa-Luc, a firefly luciferase-expressing human cervical cancer cell line, was purchased from Caliper Life Science (Hopkinton, MA). The cells were maintained in DMEM containing 10% FBS and 1% streptomycin/penicillin in a humidified atmosphere containing 5% CO_2 at 37 °C. FVB/NJc1 female mice (18–20 g, 6 weeks) were purchased from Clea Japan, Inc. (Tokyo, Japan). EL1-Luc/EL1-SV40 T-antigen transgenic mice (OncoMouse; male, 18–20 g, 6 weeks) were purchased from Caliper Life Sciences (Hopkinton, MA). Female FVB mice and male transgenic mice were allowed to breed, and the newborn mice were genotyped primarily by basal bioluminescence imaging at the age of 5 weeks. Male mice presenting basal luminescence in the pancreas were separated for use in the experiments. All animal experiments were performed in accordance with the Guidelines for the Care and Use of Laboratory Animals as stated by The University of Tokyo.

2.2. Preparation of hybrid micelles

Hybrid micelles were prepared as previously described [20]. In brief, a solution of 2.5 M $CaCl_2$ (1 μL) was diluted in 10 mM Tris buffer (pH 10) (11.5 μL). Another solution containing PEG-CCP (1.0 mg/mL) in 10 mM Tris/HCl buffer (pH 7.5) was mixed with a solution of 15 μM siRNA in 10 mM HEPES buffer (pH 7.2) and with 50 mM HEPES buffer containing 1.5

mM Na_3PO_4 and 140 mM NaCl (pH 7.5) (2.5 μL:5 μL:5 μL). The former solution was mixed with the latter solution by pipetting up and down for approximately 20 s (final siRNA concentration: 3 μM). The freshly prepared micelle solution containing 40 μg siRNA and 100 μg PEG-CCP (1 mL) was then purified and concentrated using a VivaSpin-06 device (molecular weight cut-off (MWCO): 10 kDa). The ultrafiltration was performed in a swing bucket rotor at 900 *g* and 4 °C for 20 min. To minimize non-specific binding of micelles to the membrane, the centrifuge filter devices were washed with de-ionized water before use. After centrifugation, the retained solution (100 μL) was added to 300 mM NaCl solution (100 μL) to adjust the final concentration to 150 mM NaCl. Through this procedure, the excess free calcium ions were removed from the micelle solution to the flow-through. The quantity of calcium removed was determined using a calcium sensitive dye, arsenazo III, by the SRL Laboratories (SRL Inc., Tokyo, Japan).

2.3. Transmission electron microscopic (TEM) imaging

Hybrid micelle solution (20 μL) was loaded on a 400-mesh copper grid and stained with 20 μL of uranyl acetate solution (2%, w/v) for 5 s. The copper grids with carbon-coated collodion film were glow-discharged for 10 s with an Eiko IB-3 ion coater (Eiko Engineering Co. Ltd., Japan) prior to use. The morphology of hybrid micelles was observed on a JEM-1400 (JEOL Ltd., Tokyo, Japan) with 100 kV acceleration voltage and 40 μA beam current, toward high resolution and high contrast with high performance imaging of specimens.

2.4. In vitro luciferase gene silencing

HeLa-Luc cells were seeded in a 96-well plate at a cell density of 2500 cells/well in 0.1 mL of DMEM containing 10% FBS and then pre-cultured for 24 h. Before transfection, the medium was refreshed. Hybrid micelles containing siRNA (siLuc or siScr), hybrid micelles without siRNA (mock), or naked siRNA (siLuc or siScr) were applied to each well to final siRNA concentrations of 100 and 200 nM (n = 6). After 48 h of incubation, the medium was removed and the cells were washed twice with 100 μL of PBS. The cells were then lysed with 50 μL of cell culture lysis buffer. The luciferase expression in the lysate was determined from photoluminescence intensity using the Luciferase Assay System and Mithras LB 940 (Berthold Technologies). The relative luciferase activity was calculated as a ratio to that in non-treated cells.

2.5. Biodistribution and tumor accumulation of hybrid micelles in transgenic mice

Mice were fed with alfalfa-free food *ad libitum*. A group of three male transgenic mice (15 weeks) were intravenously injected with Alexa Fluor 647-labeled siLuc (Alexa647-siLuc) contained in hybrid micelles (200 μL, 20 μg siRNA). As a control, the same amount of naked Alexa647-siLuc was also injected to another group of male transgenic mice. Intravenous injection was performed slowly (10 s per injection) to avoid adverse side effects. Mice were sacrificed 6 h after the injection, and then the main organs (heart, lungs, liver, spleen, kidneys, and pancreas, including tumors) were excised for fluorescent imaging using IVIS (Caliper Life Sciences, Hopkinton, MA). Organs were washed in PBS and kept on ice prior to analysis. Similarly, blood was collected from mice at 6 h after the injection, and then it was centrifuged at 2000 *g* for 10 min to obtain the plasma. The fluorescence intensity was determined using the Living Image software through the selection of an ROI around the whole organ/tumor and the plasma, and then it was converted to the % of dose/g of tissue (or plasma) based on a standard curve. To avoid incomplete separation of tumors from the pancreas, the combined weight of the organ and tumors was used for the subsequent statistical data analysis.

2.6. Tumor histology

After the biodistribution studies described in the preceding section were complete, a portion of the pancreas/tumor tissue from each mouse was rapidly frozen in Tissue-Tek OCT compound with liquid nitrogen in ethanol. The frozen pancreas/tumor tissues embedded in the block were then cut into 6-μm thick slices at −20 °C with a Tissue-Tek Cryo3 microtome/cryostat (Sakura Finetek USA, Inc., Torrance, CA). Each section of the pancreas/tumor tissue was fixed with formalin and stained with hematoxylin and eosin (HE) for histological identification of tumor cells and healthy pancreatic cells. In addition to HE staining, adjacent cryosections of the pancreas/tumor tissue were stained with Hoechst 33342 (Dojindo Lab., Kumamoto, Japan) for observation of cellular nuclei using a confocal laser scanning microscope (CLSM) (LSM 510, Carl Zeiss, Germany). The CLSM observation was performed at the excitation wavelengths of 633 nm (He–Ne laser) and 710 nm (MaiTai laser, two photon excitation) for Alexa647-siRNA and Hoechst 33342, respectively. The fluorescence intensities of the Alexa647-siRNA from the tumor region or the healthy pancreatic region in the obtained CLSM image were determined using the ImageJ software.

2.7. In vivo luminescence reduction in transgenic mice

Hybrid micelle solutions containing 20 μg of siLuc or siScr (200 μL) were slowly injected into the caudal vein of transgenic mice (13 weeks; n = 16). Bioluminescence intensity in the pancreatic tumors was determined before injection and 24 h after injection of the hybrid micelles using an IVIS instrument. Mice were anesthetized with isoflurane and luciferin was injected intraperitoneally at a dosage of 150 mg/kg (200 μL). Measurements were performed 10 min after luciferin injection for three different positions in each mouse (right flank, left flank, and ventral positions) to reduce variability in bioluminescence due to the tumor positions. Photons emitted from the pancreas region were quantified using the Living Image software and summed from the 3 positions. All images were set to the same conditions and color scale.

2.8. Hematological parameters and cytokine levels

Hybrid micelle solutions containing 20 μg of siScr (200 μL) were slowly injected in the caudal vein of female Balb/c mice (6 weeks). Blood was collected at several time points after the injection and centrifuged at 2000 *g* for 10 min to obtain the plasma. The levels of alkaline phosphatase (ALP), aspartate aminotransferase (AST), alanine aminotransferase (ALT), and creatinine (Cr) in the plasma were measured by the SRL Laboratories (SRL Inc., Tokyo, Japan) (n = 5). Also, the levels of tumor necrosis factor-α (TNF-α), interleukin-6 (IL-6), IL-1α, and IL-1β in plasma were determined by Quantikine® ELISA kits, according to the manufacturer's protocol (n = 4).

3. Results and discussion

3.1. Preparation of hybrid micelles

Preparation of CaP nanoparticles in an aqueous solution is known to result in the formation of insoluble large aggregates over time. Thus, PEG-CCP (Fig. 1B) was used to prepare CaP nanoparticles with enhanced colloidal stability through the steric repulsive effect of the PEG capsule. These nanoparticles also had endosome-disrupting functionality derived from the CCP segment. This segment was synthesized through the introduction of an Aco moiety into the side chain of PAsp(DET) through *cis*-aconitic amide bond formation. Successful preparation of PEG-CCP (or quantitative introduction of the Aco moiety) was confirmed using ^{1}H NMR spectroscopy (data not shown), as previously described [19]. The resulting PAsp(DET-Aco) segment was stable at neutral pH, whereas under acidic conditions, it underwent *cis*-aconitic amide cleavage to revert back to the parent PAsp(DET) (Fig. 1C) [22].

The generated PAsp(DET) enabled acidic pH-selective membrane disruption based on the distinctive change in the protonation state of the side chain unit, *i.e.*, the monoprotonated state at neutral pH and the diprotonated state at acidic pH, directed toward endosomal escape of the payload (Fig. 1C) [26,27].

The hybrid micelles were prepared by simple mixing of a solution containing PEG-CCP, siRNA, and phosphate ions, with a solution of calcium ions (Fig. 1A). The prepared micelles were then subjected to ultrafiltration (MWCO: 10 kDa) for the removal of excess free calcium ions as well as for concentration of the sample. The concentrated solution was diluted with the same volume of NaCl solution (300 mM) to generate the hybrid micelle solution at 150 mM NaCl. The obtained hybrid micelles were observed with a high performance TEM. Fig. 2A depicts spherical nanoparticles of approximately 30 nm in diameter with a clearly narrow size distribution, which was confirmed by the size distribution histogram obtained from analyses of the TEM images (mean diameter: 33.2 nm, n = 111) (Fig. 2B). The hybrid micelle solution was further characterized by dynamic light scattering (DLS) and electrophoretic light scattering. The size of hybrid micelles was 38 nm at the peak of the number-weighted histogram in DLS (Supporting Fig. S1), associated with a narrow size distribution (polydispersity index = 0.09). This size is consistent with that estimated from the TEM images. Further, the zeta-potential of hybrid micelles was almost neutral (−2.2 mV), consistent with the presence of nonionic PEG outer layer. In addition, the DLS analysis revealed that the cumulant size of the hybrid micelles was maintained over 7 days of storage at 4 °C (data not shown), demonstrating the potential for long-term storage in a refrigerator.

3.2. In vitro luciferase gene silencing

To confirm *in vitro* siRNA delivery efficacy, the hybrid micelles carrying siLuc were applied to a luciferase assay with cultured HeLa-Luc cells as a luciferase-expressing model cell line. After 48 h of incubation, siLuc delivered by the hybrid micelles significantly decreased the luciferase expression in a dose-dependent manner (Fig. 3); the hybrid micelles inhibited approximately 50% and 90% of luciferase expression at 100 nM and 200 nM siRNA, respectively. In sharp contrast, the hybrid micelles with a control sequence of siRNA (siScr) as well as the mock micelles without siRNA resulted in no reduction in luciferase expression, indicating sequence-specific, potent gene silencing ability of the hybrid micelles. In our previous studies, the hybrid micelles exhibited a significant gene silencing effect on endogenous VEGF in cultured pancreatic cancer cells (PanC-1 and BxPC3) [19,20], suggesting that their gene silencing ability is not limited to a specific target gene and cell line. The efficient gene silencing ability of the hybrid micelles was probably due to the stable encapsulation of siRNA in CaP nanoparticles in cell culture medium [20], followed by efficient cellular internalization and endosomal escape induced by the CCP segment [19]. With regard to the cellular internalization, our previous study revealed that hybrid micelles were efficiently uptaken by HeLa cells within 4 h, probably due to an energy-dependent endocytosis [16]. It should be noted that no significant cytotoxicity was observed for any of the samples at the tested concentrations, as determined in a cell viability assay using a water soluble tetrazolium salt (WST-8) (data not shown).

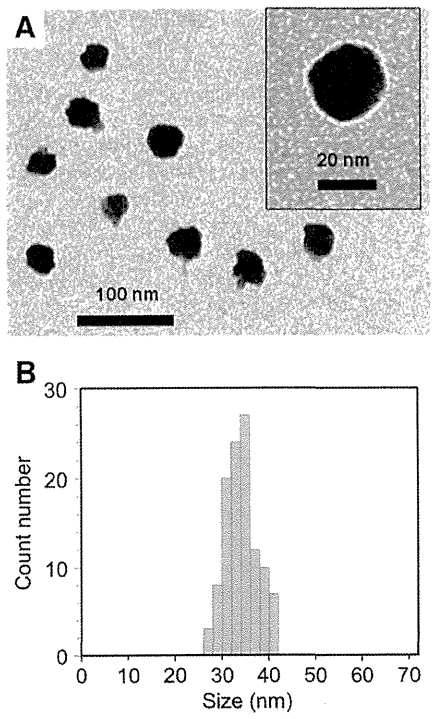

Fig. 2. (A) TEM image of the hybrid micelles. (B) Size distribution histogram of the hybrid micelles based on their TEM images.

3.3. Biodistribution and tumor accumulation of hybrid micelles in transgenic mice

Biodistribution of hybrid micelles after intravenous injection was evaluated in the transgenic mice presenting spontaneous pancreatic tumors using Alexa647-siRNA. At 6 h after injection, the transgenic mice were sacrificed, and the organs were excised for measuring fluorescence intensity, which was then converted to the % of dose/g of tissue based on a standard curve. As the border between a pancreatic tumor and healthy pancreas tissue is unclear, the fluorescence intensity of the whole pancreatic tissue was measured for tumor accumulation of Alexa647-siRNA. Note that the significant fluorescence was not detected from the collected blood samples, indicating that almost all the hybrid micelles (or Alexa647-siRNAs) were eliminated from the bloodstream within 6 h. Thus, the fluorescence intensity measured from each organ would not be affected by blood circulating micelles. As shown in Fig. 4, the amount of hybrid micelles was approximately 0.9% of dose/g of pancreas/tumor, which was 6-fold larger than that in naked siRNA. No significant difference between hybrid micelles and naked siRNA was observed for the accumulation in other organs; however, the kidneys displayed lower accumulation for Alexa647-siRNA delivered by the hybrid micelles compared to naked siRNA. These results suggest that the hybrid micelles could protect Alexa647-siRNA from rapid renal filtration, enabling it to circulate for longer in the blood, and therefore accumulate more in the pancreas/tumor.

The enhanced accumulation of hybrid micelles in the pancreas/tumor was further investigated by histological analysis. First, HE-stained sections were prepared to facilitate distinction of the tumor region (T) from healthy pancreatic tissue (H). As depicted in Fig. 5A, healthy pancreatic cells were organized into lobules toward formation of glandular acini. In contrast, tumor cells show a non-organized solid growth pattern [28,29]. Fig. 5A also shows the presence of connective tissue septa in between the T and H areas. CLSM was then performed to image the corresponding Hoechst 33342-stained sections. It is noteworthy that fluorescence signals from Alexa647-siRNA delivered by hybrid micelles were found mainly in the tumor region (Fig. 5B). Quantitative analysis using the ImageJ software indicated that the fluorescence signal of Alexa647-siRNA in the tumor region was 2.9-fold stronger than that in the healthy pancreas. By considering that the average weight of pancreas/tumor in the transgenic mice was 2.2-fold higher than that of pancreas in wild-type mice, the tumor accumulation of siRNA delivered by hybrid micelles can be roughly estimated to be ~1.3% of dose/g of tumor with the assumption that the tissue weights are similar between tumor and healthy pancreas in the transgenic mice. Thus, the

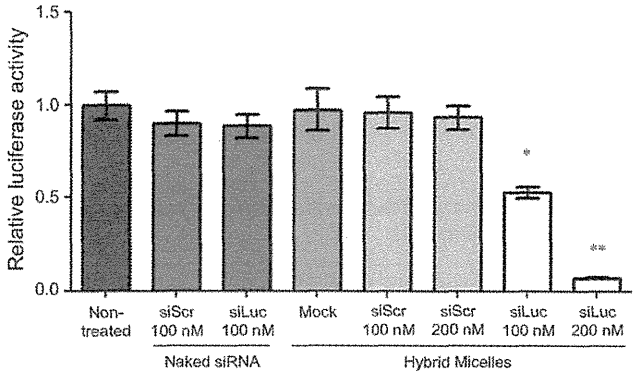

Fig. 3. *In vitro* luciferase gene silencing by hybrid micelles in cultured HeLa-Luc cells. Luciferase luminescence was quantified after 48 h of incubation of cells treated with samples. Results are expressed as mean and standard deviation (n = 6). $^{*}P < 0.05$; $^{**}P < 0.001$ (ANOVA followed by Newman–Keuls).

preferential tumor accumulation of siRNA-loaded hybrid micelles was demonstrated in the spontaneous pancreatic tumor model.

In a previous study, we reported that the tumor vasculature in the EL1-Luc/TAg transgenic mice was covered with pericytes [30], which can considerably limit the penetration of nanocarriers into the spontaneous tumor model in comparison to hypervascular and/or less stromal tumor models [31,32]. Nevertheless, the hybrid micelles apparently penetrated and distributed within the tumors (Fig. 5B). This behavior should be attributed to the relatively small size of the hybrid micelles (approximately 30–40 nm in diameter, Fig. 2 and Supporting Fig. S1), facilitating the passage of the nanocarriers through the tumor vasculature and stromal tissues. This was in agreement with our recent study where <50-nm polymeric micelles efficiently penetrated into the tissue, even in hypopermeable tumor models, which was in contrast to the control micelles that were >50 nm in size [33]. It should be further noted that the enhanced tumor accumulation behavior of hybrid micelles, compared to naked siRNA, in the present spontaneous pancreatic tumors was comparable to our previous observation in a subcutaneous BxPC3 tumor model [20]. This can also be explained by the small size of hybrid micelles, as the small-sized nanocarriers may be less affected by the tumor microenvironments restricting extravasation and penetration of nanocarriers, such as pericyte coverage of the vasculature [33]. Altogether, the hybrid micelles are a promising strategy for the systemic delivery of siRNA to various and whole tumor tissues/cells.

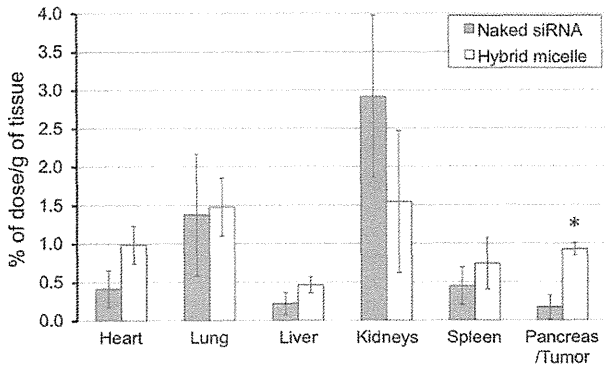

Fig. 4. Biodistribution of Alexa647-siRNA-loaded hybrid micelles and naked Alexa647-siRNA by fluorescence quantification at 6 h after intravenous injection (20 μg siRNA/injection) in 14-week-old transgenic mice. The obtained fluorescence intensities were converted to % of dose/g of tissue based on a standard curve. Results are expressed as mean and standard error of mean (n = 3). ANOVA followed by Newman–Keuls ($^{*}P < 0.01$).

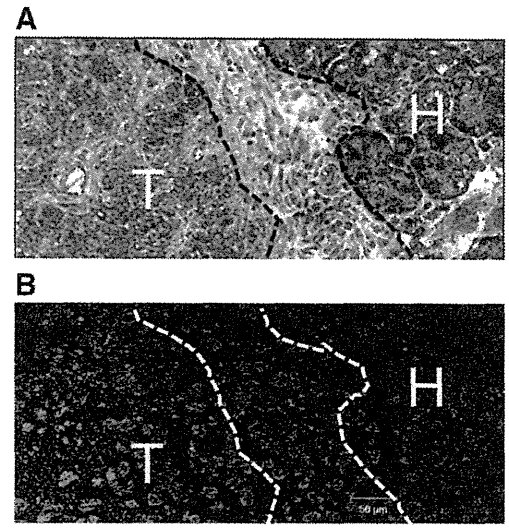

Fig. 5. Histological observation of pancreas/tumor in transgenic mice treated with hybrid micelles. Sections were prepared from the pancreas/tumor tissue excised at 6 h after intravenous injection of hybrid micelles carrying Alexa647-siRNA (20 μg siRNA/injection) to transgenic mice. (A) HE staining: non-organized tumor cells (T) and healthy pancreatic structure in lobes (H) are separated by the dotted line. (B) CLSM image of an adjacent section to that stained with HE. Nuclei (blue) were stained with Hoechst 33342, and Alexa647-siRNA is shown in green.

3.4. *In vivo* luciferase gene silencing in transgenic mice

Pancreatic cancer is considered to be one of the most fatal cancers [34]. Moreover, the all-stage 5-year survival has not improved greatly during the last 25 years [35]. These facts have motivated us to develop novel therapeutics to improve the prognosis of pancreatic cancer patients. An immunocompetent mouse presenting spontaneous pancreatic tumors is a useful model for establishment of such novel therapeutics, including anticancer drug-loaded micelles [30]. Herein, the *in vivo* gene silencing activity of hybrid micelles was evaluated with the spontaneous pancreatic tumor model developed in EL1-Luc/TAg transgenic mice, in which the expression of firefly luciferase is promoted specifically in the acinar cell carcinoma [25]. Accordingly, this model can be used for a gene silencing assay that employs the bioluminescence of the pancreatic tumors. It is worth noting that the following characteristics were confirmed for the spontaneous pancreatic cancer model in the previous study [30]; i) liver and intestine metastases are likely to occur in this model after the mice becoming 16 weeks old, ii) the pancreas/tumor in this model is enlarged and also the pancreatic cancer may grow over the normal position of pancreas, and iii) the bioluminescent signal from the pancreatic cancer is not always emitted from the same anatomic position. Considering these points, the bioluminescence measurements in this study were performed for 3 different positions, *i.e.*, left flank, frontal, and right flank of the 13-week-old mice without detectable tumor metastases.

Representative bioluminescence images of the left flank position of mice treated with or without siLuc-loaded hybrid micelles are shown in Fig. 6A, where the variable bioluminescence signals from the pancreatic tumor can be identified. At 24 h after systemic injection of the hybrid micelles, the bioluminescence intensity in the pancreatic tumors exhibited a significant reduction of 61% compared with the initial intensity before injection (Fig. 6B; $P < 0.01$), indicating that the hybrid micelles induced efficient luciferase gene silencing in the tumor tissue. There was no significant reduction in the bioluminescence signal after injection of siScr-loaded hybrid micelles, indicating that the reduction in the bioluminescence intensity was due to the sequence-specific

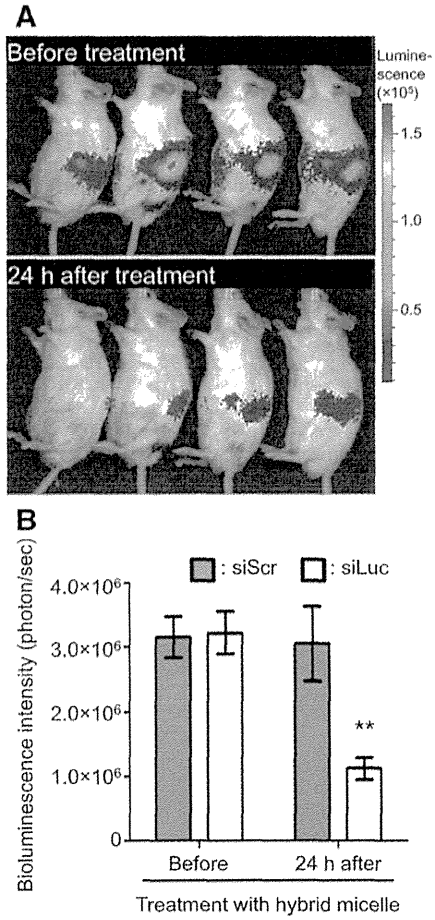

Fig. 6. *In vivo* gene silencing activity of systemically administered hybrid micelles in the spontaneous pancreatic tumors of transgenic mice. (A) Representative images of mice before and 24 h after injection of hybrid micelles containing siLuc (20 μg siRNA/mouse). (B) Bioluminescence intensity in the pancreatic tumors after intravenous injection of hybrid micelles containing siLuc or siScr (20 μg siRNA/mouse). Results are expressed as mean and standard deviation (n = 16). ANOVA followed by Newman–Keuls (**$P < 0.01$).

RNAi machinery. The similar gene silencing profile of hybrid micelles was further observed for the protein amount of luciferase in homogenized pancreas/tumor tissues (Supporting Fig. S2). This sequence-specific gene silencing activity of hybrid micelles is consistent with their significantly enhanced tumor accumulation of the siRNA payload (Figs. 4 and 5), which was roughly estimated to be ~1.3% of dose/g of tumor, corresponding to ~40 ng siRNA. Interestingly, the *in vivo* gene silencing efficacy of hybrid micelles in the spontaneous pancreatic cancer cells (60% with ~40 ng siRNA) was apparently higher than the *in vitro* efficacy in the cultured HeLa-Luc cells (50% with ~130 ng siRNA). These different efficacies might be due to varying cellular innate functions between the *in vivo* pancreatic cancer cells and the *in vitro* monolayer-cultured cervical cancer cells. The cellular innate functions, including the expression levels of luciferase and RNAi-related genes, are known to be substantially altered between live tissue and cell culture, especially monolayer culture, and also different types of cells [36–38]. Indeed, the luciferase expression in the present pancreatic cancer cells was lost in monolayer culture. This is the reason for the use of HeLa-Luc cells as a conventional cancer cell line for demonstrating the *in vitro* gene silencing activity of hybrid micelles.

3.5. Hematological parameters and cytokine levels after systemic administration of hybrid micelles

To verify the safety of the hybrid micelle formulation, hematological parameters and inflammatory cytokine levels were measured at several time points after systemic administration. As summarized in Table 1, the intravenous injection of hybrid micelles induced no remarkable changes in the levels of AST, ALT, and ALP as indicators of liver function and that of Cr as an indicator of kidney function over 48 h, suggesting negligible adverse side effects on the liver and the kidneys. Similarly, the levels of inflammatory cytokines, *i.e.*, TNF-α, IL-6, IL-1α, and IL-1β, were not affected by the injection of hybrid micelles (Supporting Fig. S3). Overall, it was demonstrated that the intravenous injection of hybrid micelles induced no severe acute toxicity under the tested conditions.

4. Conclusion

In the present study, hybrid micelles prepared with a smart block copolymer PEG-CCP were applied for systemic siRNA delivery to spontaneous pancreatic tumors in EL1-Luc/TAg transgenic mice. The obtained results confirmed the enhanced accumulation of siRNA-loaded hybrid micelles in the tumor tissue and their significant gene silencing activity. Notably, this was associated with negligible changes in hematological parameters. Altogether, the great potential of the hybrid micelles for RNAi-based cancer therapy was successfully demonstrated.

Acknowledgment

This research was funded by the Japan Society for the Promotion of Science (JSPS) through the "Funding Program for World-Leading Innovative R&D on Science and Technology (FIRST Program)," the Adaptable and Seamless Technology Transfer Program through Target-driven R&D (A-STEP), the National Institute of Biomedical Innovation (NIBIO), and Grants-in-Aid for Scientific Research from the Japanese Ministry of Health, Labour and Welfare. Part of this work was conducted in the Research Hub for Advanced Nano Characterization, The University of Tokyo, supported by the Ministry of Education, Culture, Sports, Science and Technology (MEXT), Japan. The authors are grateful to S. Ogura and K. Date for their assistance with animal care.

Appendix A. Supplementary data

Supplementary data to this article can be found online at http://dx.doi.org/10.1016/j.jconrel.2014.01.008.

References

[1] A. Fire, S. Xu, M.K. Montgomery, S.A. Kostas, S.E. Driver, C.C. Mello, Potent and specific genetic interference by double-stranded RNA in *Caenorhabditis elegans*, Nature 391 (1998) 806–811.

Table 1
Hematological parameters after intravenous injection of hybrid micelles (20 μg siRNA/mouse).

	Non-treated (0 min)	10 min	30 min	60 min	120 min	20 h	48 h
AST (U/L)	40 ± 5	38 ± 9	42 ± 4	40 ± 5	41 ± 5	36 ± 4	47 ± 7
ALT (U/L)	61 ± 18	62 ± 13	73 ± 5	67 ± 8	64 ± 12	86 ± 28	61 ± 23
ALP (U/L)	401 ± 25	401 ± 22	424 ± 10	378 ± 8	384 ± 23	377 ± 28	477 ± 37
Cr (mg/dL)	0.11 ± 0.01	0.11 ± 0.01	0.11 ± 0.01	0.10 ± 0.01	0.10 ± 0.01	0.10 ± 0.02	0.07 ± 0.01

Abbreviations: AST, aspartate aminotransferase; ALT, alanine aminotransferase; ALP, alkaline phosphatase; Cr, creatinine. Results are expressed as mean and standard deviation (n = 5).

[2] S.M. Elbashir, J. Harborth, W. Lendeckel, A. Yalcin, K. Weber, T. Tuschl, Duplexes of 21-nucleotide RNAs mediate RNA interference in cultured mammalian cells, Nature 411 (2001) 494–498.
[3] K. Whitehead, R. Langer, D. Anderson, Knocking down barriers: advances in siRNA delivery, Nat. Rev. Drug Discov. 8 (2009) 129–138.
[4] J.C. Burnett, J.J. Rossi, RNA-based therapeutics: current progress and future prospects, Chem. Biol. 19 (2012) 60–71.
[5] F. Takeshita, T. Ochiya, Therapeutic potential of RNA interference against cancer, Cancer Sci. 97 (2006) 689–696.
[6] Y.-K. Oh, T.G. Park, siRNA delivery systems for cancer treatment, Adv. Drug Deliv. Rev. 61 (2009) 850–862.
[7] F. van de Water, O. Boerman, A. Wouterse, J. Peters, F. Russel, R. Masereeuw, Intravenously administered short interfering RNA accumulates in the kidney and selectively suppresses gene function in renal proximal tubules, Drug Metab. Dispos. 34 (2006) 1393–1397.
[8] J. Turner, S. Jones, S. Moschos, M. Lindsay, M. Gait, MALDI-TOF mass spectral analysis of siRNA degradation in serum confirms an RNase A-like activity, Mol. Biosyst. 3 (2007) 43–50.
[9] R.J. Christie, N. Nishiyama, K. Kataoka, Delivering the code: polyplex carriers for deoxyribonucleic acid and ribonucleic acid interference therapies, Endocrinology 151 (2010) 466–473.
[10] C.A. Chen, H. Okayama, Calcium phosphate-mediated gene-transfer—a highly efficient transfection system for stably transforming cells with plasmid DNA, Biotechniques 6 (1988) 632.
[11] M. Jordan, A. Schallhorn, F.M. Wurm, Transfecting mammalian cells: optimization of critical parameters affecting calcium-phosphate precipitate formation, Nucleic Acids Res. 24 (1996) 596–601.
[12] Y. Kakizawa, K. Kataoka, Block copolymer self-assembly into monodispersive nanoparticles with hybrid core of antisense DNA and calcium phosphate, Langmuir 18 (2002) 4539–4543.
[13] M. Zhang, K. Kataoka, Nano-structured composites based on calcium phosphate for cellular delivery of therapeutic and diagnostic agents, Nano Today 4 (2009) 508–517.
[14] J. Li, Y.C. Chen, Y.C. Tseng, S. Mozumdar, L. Huang, Biodegradable calcium phosphate nanoparticle with lipid coating for systemic siRNA delivery, J. Control. Release 142 (2010) 416–421.
[15] Y. Kakizawa, K. Miyata, S. Furukawa, K. Kataoka, Size-controlled formation of a calcium phosphate-based organic–inorganic hybrid vector for gene delivery using poly(ethylene glycol)-block-poly(aspartic acid), Adv. Mater. 16 (2004) 699–702.
[16] Y. Kakizawa, S. Furukawa, K. Kataoka, Block copolymer-coated calcium phosphate nanoparticles sensing intracellular environment for oligodeoxynucleotide and siRNA delivery, J. Control. Release 97 (2004) 345–356.
[17] Y. Kakizawa, S. Furukawa, A. Ishii, K. Kataoka, Organic–inorganic hybrid-nanocarrier of siRNA constructing through the self-assembly of calcium phosphate and PEG-based block aniomer, J. Control. Release 111 (2006) 368–370.
[18] M. Zhang, A. Ishii, N. Nishiyama, S. Matsumoto, T. Ishii, Y. Yamasaki, K. Kataoka, PEGylated calcium phosphate nanocomposites as smart environment-sensitive carriers for siRNA delivery, Adv. Mater. 21 (2009) 3520–3525.
[19] F. Pittella, M. Zhang, Y. Lee, H.J. Kim, T. Tockary, K. Osada, T. Ishii, K. Miyata, N. Nishiyama, K. Kataoka, Enhanced endosomal escape of siRNA-incorporating hybrid nanoparticles from calcium phosphate and PEG-block charge-conversional polymer for efficient gene knockdown with negligible cytotoxicity, Biomaterials 32 (2011) 3106–3114.
[20] F. Pittella, K. Miyata, Y. Maeda, T. Suma, Q. Chen, R.J. Christie, K. Osada, N. Nishiyama, K. Kataoka, Pancreatic cancer therapy by systemic administration of VEGF siRNA contained in calcium phosphate/charge-conversional polymer hybrid nanoparticles, J. Control. Release 161 (2012) 868–874.
[21] H. Takemoto, K. Miyata, S. Hattori, T. Ishii, T. Suma, S. Uchida, N. Nishiyama, K. Kataoka, Acidic pH-responsive siRNA conjugate for reversible carrier stability and accelerated endosomal escape with reduced IFNα-associated immune response, Angew. Chem. Int. Ed. 52 (2013) 6218–6221.
[22] Y. Lee, K. Miyata, M. Oba, T. Ishii, S. Fukushima, M. Han, H. Koyama, N. Nishiyama, K. Kataoka, Charge conversion ternary polyplex with endosomes disruption moiety: a technique for efficient and safe gene delivery, Angew. Chem. Int. Ed. 120 (2008) 5241–5244.
[23] K.K. Frese, D.A. Tuveson, Maximizing mouse cancer models, Nat. Rev. Cancer 7 (2007) 654–658.
[24] G. Francia, W. Cruz-Munoz, S. Man, P. Xu, R.S. Kerbe, Mouse models of advanced spontaneous metastasis for experimental therapeutics, Nat. Rev. Cancer 11 (2011) 135–141.
[25] N. Zhang, S. Lyons, E. Lim, P. Lassota, A spontaneous acinar cell carcinoma model for monitoring progression of pancreatic lesions and response to treatment through noninvasive bioluminescence imaging, Clin. Cancer Res. 15 (2009) 4915–4924.
[26] K. Miyata, M. Oba, M. Nakanishi, S. Fukushima, Y. Yamasaki, H. Koyama, N. Nishiyama, K. Kataoka, Polyplexes from poly(aspartamide) bearing 1,2-diaminoethane side chains induce pH-selective, endosomal membrane destabilization with amplified transfection and negligible cytotoxicity, J. Am. Chem. Soc. 130 (2008) 16287–16294.
[27] K. Miyata, N. Nishiyama, K. Kataoka, Rational design of smart supramolecular assemblies for gene delivery: chemical challenges in the creation of artificial viruses, Chem. Soc. Rev. 41 (2012) 2562–2574.
[28] L.A. Aaltonen, S.R. Hamilton, World Health Organization; international agency for research on cancer, in: L.A. Aaltonen, S.R. Hamilton (Eds.), Pathology and Genetics of Tumours of the Digestive System, IARC Press: Oxford University Press, Lyon: Oxford, 2000, (314 pp.).
[29] R.A. Caruso, A. Inferrera, G. Tuccari, G. Barresi, Acinar cell carcinoma of the pancreas, a histologic, immunocytochemical and ultrastructural study, Histol. Histopathol. 9 (1994) 53–58.
[30] H. Cabral, M. Murakami, H. Hojo, Y. Terada, M.R. Kano, U.-I. Chung, N. Nishiyama, K. Kataoka, Targeted therapy of spontaneous murine pancreatic tumors by polymeric micelles prolongs survival and prevents peritoneal metastasis, Proc. Natl. Acad. Sci. U. S. A. 110 (2013) 11397–11402.
[31] M.R. Kano, Y. Bae, C. Iwata, Y. Morishita, M. Yashiro, M. Oka, T. Fujii, A. Komuro, K. Kiyono, M. Kaminishi, K. Hirakawa, Y. Ouchi, N. Nishiyama, K. Kataoka, K. Miyazono, Improvement of cancer-targeting therapy, using nanocarriers for intractable solid tumors by inhibition of TGF-β signaling, Proc. Natl. Acad. Sci. U. S. A. 104 (2007) 3460–3465.
[32] L. Zhang, H. Nishihara, M.R. Kano, Pericyte-coverage of human tumor vasculature and nanoparticle permeability, Biol. Pharm. Bull. 35 (2012) 761–766.
[33] H. Cabral, Y. Matsumoto, K. Mizuno, Q. Chen, M. Murakami, M. Kimura, Y. Terada, M.R. Kano, K. Miyazono, M. Uesaka, N. Nishiyama, K. Kataoka, Accumulation of sub-100 nm polymeric micelles in poorly permeable tumours depends on size, Nat. Nanotechnol. 6 (2011) 815–823.
[34] American Cancer Society, Cancer Facts & Figs. 2011, Epidemiologic Surveillance Report, American Cancer Society, Atlanta, 2011, (available at: <http://www.cancer.org/acs/groups/content/@epidemiologysurveilance/documents/document/acspc-029771.pdf>. Accessed April 2013).
[35] A. Jemal, R. Siegel, J. Xu, E. Ward, Cancer statistics, 2010, CA Cancer J. Clin. 260 (2010) 277–300.
[36] F. Pampaloni, E.G. Reynaud, E.H.K. Stelzer, The third dimension bridges the gap between cell culture and live tissue, Nat. Rev. Mol. Cell Biol. 8 (2007) 839–845.
[37] N.J. Yoo, S.Y. Hur, M.S. Kim, J.Y. Lee, S.H. Lee, Immunohistochemical analysis of RNA-induced silencing complex-related proteins AGO2 and TNRC6A in prostate and esophageal cancers, APMIS 118 (2010) 271–276.
[38] T. Endo, K. Itaka, M. Shioyama, S. Uchida, K. Kataoka, Gene transfection to spheroid culture system on micropatterned culture plate by polyplex nanomicelle: a novel platform of genetically-modified cell transplantation, Drug Deliv. Transl. Res. 2 (2012) 398–405.

Carcinogenesis vol.35 no.5 pp.1003–1011, 2014
doi:10.1093/carcin/bgt402
Advance Access publication December 6, 2013

Macrophage-derived reactive oxygen species suppress miR-328 targeting CD44 in cancer cells and promote redox adaptation

Takatsugu Ishimoto†, Hidetaka Sugihara†, Masayuki Watanabe, Hiroshi Sawayama, Masaaki Iwatsuki, Yoshifumi Baba, Hirohisa Okabe, Kosei Hidaka, Naomi Yokoyama, Keisuke Miyake, Momoko Yoshikawa[1], Osamu Nagano[1], Yoshihiro Komohara[2], Motohiro Takeya[2], Hideyuki Saya[1] and Hideo Baba*

Department of Gastroenterological Surgery, Graduate School of Medical Science, Kumamoto University, 1-1-1 Honjo, Kumamoto 860–8556, Japan, [1]Division of Gene Regulation, Institute for Advanced Medical Research, School of Medicine, Keio University, 35 Shinanomachi, Shinjuku-ku, Tokyo 160–8582, Japan and [2]Department of Cell Pathology, Graduate School of Medical Science, Kumamoto University, 1-1-1 Honjo, Kumamoto 860–8556, Japan

*To whom correspondence should be addressed. Tel: +81 96 373 5212; Fax: +81 96 371 4378; Email: hdobaba@kumamoto-u.ac.jp

CD44 is frequently overexpressed in a wide variety of epithelial malignancies including gastrointestinal cancer and causes resistance to currently available treatments. MicroRNAs (miRNAs) are non-coding RNAs that regulate molecular pathways in cancer by targeting various genes. The aim of this study was to investigate the regulation of CD44 expression by miRNAs and to develop new molecular targets in gastrointestinal cancer. We performed miRNA screening in six human gastrointestinal cancer cell lines and identified three candidate miRNAs that could regulate CD44 expression in gastrointestinal cancer. Among these, we focused on miR-328 and examined its functional relevance using growth assays and cytotoxicity assays. CD44 expression was reduced in gastrointestinal cancer cell lines forced to express miR-328, leading to inhibition of cancer cell growth *in vitro* and *in vivo*, and impaired resistance to chemotherapeutic drugs and reactive oxygen species (ROS). In contrast, induction of CD44 expression by miR-328 inhibitor led to promotion of cancer cell growth. Furthermore, we revealed that ROS produced by macrophages triggered CD44 expression through suppression of miR-328 in gastric cancer cells. Finally, tumor-infiltrating macrophages (CD68 and CD163) were closely related to both miR-328 downregulation and CD44 upregulation in 63 patients with surgically resected gastric cancer. These findings suggest that macrophages in the tumor microenvironment may cause increased CD44 expression through miR-328 suppression, resulting in tumor progression by enhancing ROS defense. miR-328-CD44 signaling mediated by macrophages may thus represent a potential target for the treatment of gastrointestinal cancer.

Introduction

Increasing evidence has recently shown that cancer stem cells (CSCs) possess an enhanced tumor-initiating capacity, and are implicated in tumor progression and metastasis. CD44 has been identified as one of the cell surface markers associated with CSCs in several tumor types (1–3) and has been implicated in a variety of physiological processes in addition to cancer cell invasion and metastasis. CD44 is synthesized in multiple isoforms as a result of alternative messenger RNA (mRNA) splicing (4,5). We previously demonstrated abundant expression of the CD44 variant isoform (CD44v) and its association with the progression of mouse gastric tumors and human gastrointestinal malignancies (6,7). Furthermore, we reported that CD44v contributed to reactive oxygen species (ROS) defense by promoting the synthesis of the primary intracellular antioxidant glutathione. CD44v interacts with and stabilizes xCT, a subunit of the glutamate–cystine transporter, thereby promoting the uptake of cystine for glutathione synthesis and resulting in the proliferation of gastric tumor cells (8).

MicroRNAs (miRNAs) are non-coding RNAs (20–22 nucleotides long), which repress mRNA translation by base pairing to partially complimentary sequences in the 3′-untranslated region (UTR) of their target mRNAs. These non-coding RNAs have the potential to post-transcriptionally regulate ~30% of all human genes (9). Emerging evidence suggests that dysregulation of miRNAs is involved in the pathogenesis of many cancers, and that the network of miRNAs regulates CSC properties (10,11). However, the mechanisms underlying the regulation of CSC properties by miRNAs are largely unknown.

Solid tumors consist of cancer cells and various types of stromal cells, fibroblasts, endothelial cells and hematopoietic cells, mainly macrophages and lymphocytes. Monocytes recruited from the circulation differentiate into mature macrophages within the tumor microenvironment. Macrophages comprise the most abundant immune population in the tumor microenvironment and are responsible for the production of cytokines, chemokines and toxic intermediates such as nitric oxide and ROS. Macrophages have functional plasticity and can change their phenotype in response to various environmental factors. There are two different states of polarized macrophage activation: classically activated (M1) and alternatively activated (M2) macrophage phenotypes. Recent studies determined that M1- and M2-polarized macrophages play different functional roles in the tumor microenvironment (12,13). M1-polarized macrophages are generally considered to act as host defense effector cells, which protect the body against attack by pathogens and tumor cells. In contrast, M2-polarized macrophages are thought to contribute to tumor growth, tumor angiogenesis, extravasation of tumor cells and suppression of antitumor immunity in various types of cancers. However, more recent studies have demonstrated that macrophages show considerable diversity and plasticity, and the phenotypes of M1- and M2-polarized macrophages can be reversed under diverse pathological conditions (14,15).

It has been reported that a local inflammatory response is responsible for increased expression of CD44 and its variant CD44 v9 (16), but no precise mechanism of CD44 upregulation has yet been determined. We suspected that the miRNA network and inflammatory cells in the tumor microenvironment may be key factors in the mechanism of CD44 upregulation in gastrointestinal cancer tissues.

In this study, we investigated the role of miR-328 in the regulation of CD44 expression in gastrointestinal cancer cells, and examined the relationship between macrophages in the tumor microenvironment and the downregulation of miR-328 and upregulation of CD44. Here, we show that macrophages may promote gastric cancer progression by downregulating miR-328 and upregulating CD44, thus identifying a potential new target for gastric cancer treatments.

Abbreviations: CSCs, cancer stem cells; CD44v, CD44 variant isoform; FACS, fluorescence-activated cell sorting; IHC, immunohistochemistry; IL, interleukin; mRNA, messenger RNA; miRNAs, microRNAs; NAC, *N*-acetylcysteine; PMA, phorbol myristate acetate; qRT–PCR, quantitative real-time reverse transcription–PCR; ROS, reactive oxygen species; siRNA, small interfering RNA; TNF, tumor necrosis factor; UTR, untranslated region.

†These authors contributed equally to this work.

Materials and methods

Cell culture and treatment

The cancer cell lines AGS, KATOIII, NUGC4, HT29 and COLO201 were cultured in 5% CO_2 at 37°C in RPMI 1640 supplemented with 10% fetal

bovine serum. HCT116 cancer cells were cultured under 5% CO_2 at 37°C in Dulbecco's modified Eagle's medium-nutrient mixture F-12 (Sigma, St Louis, MO) supplemented with 10% fetal bovine serum. These cell lines were obtained from the Japanese Collection of Research Bioresources Cell Bank and Riken BioResource Center Cell Bank.

RNA and miRNA isolation

Total RNA, including miRNA, was isolated from cell lines using a mirVana miRNA Isolation Kit (Ambion, Austin, TX) and finally eluted into 100 μl of heated elution solution, according to the manufacturer's protocol. miRNAs were extracted from formalin-fixed, paraffin-embedded normal gastric epithelium and gastric cancer tissues using a RecoverAll Total Nucleic Acid Isolation Kit for FFPE (Ambion), according to the manufacturer's instructions. The purity and concentration of all RNA samples were evaluated by their absorbance ratio at 260/280 nm, determined using a NanoDrop ND-1000 spectrophotometer (NanoDrop Technologies, Rockland, DE).

miRNA PCR array

miRNA expression was analyzed using the Human miFinder 384HC miScript miRNA PCR Array, which profiles the expression of the 372 most abundantly expressed and best characterized miRNAs in miRBase, according to the manufacturer's instructions.

Quantitative real-time reverse transcription–PCR

The expression levels of miR-328 were determined by TaqMan quantitative real-time reverse transcription–PCR (qRT–PCR) using TaqMan miRNA assay kits (Ambion), according to the manufacturer's protocol, as described previously. miR-328 expression was normalized to that of RNU6B small nuclear RNA expression. Expression levels of CD44 were quantified by SYBR Green qRT–PCR using a LightCycler 480 SYBR Green I Master (Roche Diagnostics, Mannheim, Germany) and normalized to glyceraldehyde-3-phosphate dehydrogenase. All qRT–PCR reactions were run using the LightCycler 480 System II (Roche Diagnostics). The relative amounts of miR-328 and CD44 were measured with the $2^{-\Delta\Delta CT}$ method. All qRT–PCR reactions were performed in triplicate.

Transfection of miRNA

Cells were transfected with 5 nM mimic or inhibitory miR-328 (Applied Biosystems, Foster City, CA) using Lipofectamine 2000 or RNAiMax transfection reagent (Invitrogen, Carlsbad, CA), according to the manufacturer's instructions. The specificity of the transfection was verified using a negative control mimic (Applied Biosystems). The expression levels of miR-328 were quantified 24 and 48 h after transfection, and the cells were used for subsequent experiments.

Generation of wild-type and mutant CD44 3′-UTR

We predicted three candidate sites in the CD44 3′-UTR, which might be directly bound by miR-328, using the miRanda algorithm. Oligonucleotide pairs (Supplementary Table S2, available at *Carcinogenesis* Online) containing the miR-328-targeting sequences of human CD44 3′-UTR and the overhangs of restriction sites were annealed. Vectors containing mutated miR-328-targeting sequences of human CD44 3′-UTR were introduced by site-directed mutagenesis primers. A luciferase reporter vector was generated by these oligonucleotide pairs ligated into the linearize the pmirGLO Dual-Luciferase miRNA Target Expression Vector (Promega: E1330) by *Dra*I (TaKaRa: 1037A) and *Nhe*I (TaKaRa: 1241A).

Luciferase assay

HCT116 cells in 96-well plates were transfected with MultiFectam (Promega: ETF5000) using the pmirGLO Dual-Luciferase miRNA Target Expression Vector (Promega: E1330) containing firefly luciferase and renilla luciferase, and Luc-CD44-a, aM, b, bM, c, cM or control (non-insert), and mimic NC (negative control) or mimic miR-328 (Invitrogen). Reporter assays were performed at 48 h after transfection, firefly and renilla luciferase activities using Dual-Glo™ Luciferase Assay System (Promega: E2940). All transfection experiments were conducted in triplicate.

Cell isolation and fluorescence-activated cell sorting analysis

Cultured cells were dissociated by exposure to Accutase. Single cell suspensions were incubated with antibodies for 30 min at 4°C for flow cytometry and fluorescence-activated cell sorting (FACS). Fluorescein isothiocyanate-conjugated antibodies to CD44 were obtained from BD. Apoptotic cells were excluded during FACS by eliminating cells that stained positive for 7-aminoactinomycin D (BD Biosciences, Tokyo, Japan). Flow cytometric analysis and FACS were performed using a BD FACSVerse flow cytometer and a BD FACSAria™ II Cell Sorter (BD), respectively.

Plasmids and siRNA transfection

A complementary DNA encoding full-length human CD44v8-10 was constructed as described previously (17). Complementary DNAs for human CD44v8-10 were introduced into the pRc/CMV expression plasmid (Invitrogen, Tokyo, Japan), and HCT116 cells were transfected with the resulting vectors using Lipofectamine LTX reagents (Invitrogen). The sequences of the small interfering RNA (siRNA; chimeric RNA–DNA) duplexes (Japan Bioservice, Saitama, Japan) were as follows: CD44, 5′-AAAUGGUCGCUACA GCAUCTT-3′ and 5′-GAUGCU GUAGCGACCAUUUTT-3′; luciferase (GL-2, control), 5′-CGUACGCGGAAUACU UCGATT-3′ and 5′-UCGA AGUAUUCCGCGUACGTT-3′. Cells were transfected with the annealed siRNAs for 24–72 h using Lipofectamine RNAi MAX reagent (Invitrogen).

Stable miR-328 overexpression and in vivo tumorigenicity assay

An expression vector encoding miR-328 was constructed and introduced into the BLOCK-iT™ Pol II miR RNAi Expression Vector Kit with EmGFP (Invitrogen). HCT116 cells were transfected with the resulting vectors using Lipofectamine LTX reagents (Invitrogen). Cells stably expressing miR-328 were obtained by selection with 5 μg/μl blasticidin for 2 weeks and then isolated by FACS based on EmGFP expression. Six-week-old nude mice (Balb-nu/nu slc) were inoculated subcutaneously in the right flank with HCT116 cells (1×10^6) stably expressing control or miR-328 vector in 100 ml phosphate-buffered saline containing 50% Matrigel (BD). All animal procedures and care were approved by the animal care and use committee of Kumamoto University.

Western blot analysis

Cultured cells collected from six-well plates were washed once in phosphate-buffered saline and lysed in radioimmunoprecipitation buffer supplemented with protease/phosphatase inhibitor cocktail (Thermo Scientific, Tokyo, Japan). Each protein sample was subjected to sodium dodecyl sulfate–polyacrylamide gel electrophoresis, transferred to a nitrocellulose membrane and exposed to primary antibodies. Signals were detected by incubation with secondary antibodies labeled using the Enhanced Chemiluminescence Detection System (GE Healthcare, Little Chalfont, UK).

Immunohistochemistry and scoring

Sample processing and immunohistochemistry (IHC) procedures were performed as described in a previous report (8). Endogenous peroxidase activity was blocked using 3% hydrogen peroxide. The sections were incubated with diluted antibodies and then with a biotin-free horseradish peroxidase-labeled polymer from the Envision Plus detection system (Dako, Glostrup, Denmark). Positive reactions were visualized using diaminobenzidine solution, followed by counterstaining with Meyer's hematoxylin. All IHC staining was scored independently by two pathologists. The membranous CD44v9, cytoplasmic CD68 and CD163 expressions were interpreted according to the guidelines published in previous studies (18,19). For membranous CD44v9, cytoplasmic CD68 and CD163, we graded the results into categories from 0 to 3+ as follows: membrane and cytoplasmic expressions were scored as: 0, no staining; 1+, 1–25%; 2+, 26–50% and 3+, >50% of the specimen stained. A score of 3+ was considered to be a positive IHC result.

Antibodies for IHC and immunoblotting analyses

For IHC, human CD44 was detected using a previously generated rat monoclonal antibody specific for human CD44v9 (1:100) (8). Human CD68 was detected using a mouse monoclonal antibody specific for human CD68 (1:100 dilution; Dako). Human CD163 was detected using a mouse monoclonal antibody specific for human CD163 (1:100 dilution; Novocastra, Newcastle, UK). For immunoblot analysis, human CD44 was detected using previously generated rabbit polyclonal antibodies to CD44cyto (1:1000) (17). Human β-catenin was detected with a rabbit monoclonal antibody for human β-catenin (1:1000; Cell Signaling Technology, Tokyo, Japan). Human β-actin was detected with a rabbit polyclonal antibody for human β-actin (1:1000; Cell Signaling Technology).

Measurement of ROS

Cells were incubated with 10 μM 2′,7′-dichlorofluorescein diacetate for 15 min at 37°C, washed twice with phosphate-buffered saline and subjected to fluorescence microscopy in images acquired with a Biorevo BZ-9000 fluorescence microscope (Keyence, Tokyo, Japan) and analysis software.

Cell proliferation assay

Cell proliferation assays were carried out in 96-well plates using the WST-8 assay with a Cell Counting Kit-8 (Dojindo Laboratories, Kumamoto, Japan) at 24, 48, 72 and 96 h after transfection, according to the manufacturer's instructions. Absorbance was measured at 450 nm.

In vitro cytotoxicity assay

HCT116 cells transfected with control or mimic miR-328 were plated in 96-well microplates (2×10^3 cells per well), cultured overnight and then exposed to H_2O_2 or cisplatin (CDDP) in triplicate for 3 days. The number

of viable cells was then determined using a Cell Counting Kit-8 (Dojindo Laboratories). Each IC_{50} value was determined as the concentration of test agent for which test luminescence/control luminescence (T/C) equaled 50%.

THP-1 macrophage preparation and co-culture assay

For M1-polarized THP-1 macrophages, 320 nM phorbol myristate acetate (PMA) was added to THP-1 cells for 6 h, followed by PMA plus 20 ng/ml interferon γ and 100 ng/ml lipopolysaccharide for the following 18 h. For M2-polarized THP-1 macrophages, 320 nM PMA was added to THP-1 cells for 6 h, followed by PMA plus 20 ng/ml interleukin (IL)-4/IL-13 for the following 18 h. After three washes to remove cytokines, M1- or M2-polarized THP-1 macrophages (upper inserts) were co-cultured with AGS cells (in six-well plates, 2×10^5 cells per well) without direct contact. After 24 h of co-culture, the upper inserts containing macrophages were discarded and the AGS cells were washed and used for subsequent experiments.

Patients and tissue samples

Primary gastric carcinoma tissue and matched normal gastric epithelium were obtained from 63 patients who underwent gastric resection without preoperative treatment at the Department of Gastroenterological Surgery, Kumamoto University Hospital from 2005 to 2008, after receiving adequate informed consent. The study was approved by the medical ethics committee of Kumamoto University.

Statistical analysis

All experiments were performed in triplicate and the data shown are representative of consistently observed results. Data are presented as the mean ± SD. Independent Student's *t*-tests were used to compare continuous variables between the two groups. Data were analyzed using JMP (SAS Institute, Tokyo, Japan) and Excel 2007 (Microsoft, Redmond, WA). A *P*-value of <0.05 was considered statistically significant.

Results

Identification of miRNAs regulating CD44 expression using cancer-related-miRNA screening in gastrointestinal cancer cells

CD44 is a cell surface marker for CSCs and is involved in the regulation of CSC ability. We recently reported that CD44 played a functional role in ROS defense and caused tumor development in gastrointestinal cancer (8). CD44 expression is regulated by Wnt β-catenin signaling in the intestine (20). We, therefore, examined CD44 and β-catenin expression in three gastric cancer lines (AGS, NUGC4 and KATOIII) and three colorectal cancer lines (COLO201, HT29 and HCT116) by western blotting. There was a negative association between CD44 and β-catenin expression (Figure 1A). Several miRNAs are implicated in regulating the abilities of CSCs, including self-renewal, tumorigenicity and chemoresistance (11). We, therefore, tested the hypothesis that the regulation of CD44 expression in gastrointestinal cancer cells may be mediated by miRNAs using miRNA qRT–PCR array analysis. We selected 59 miRNAs that were down-regulated by less than half in high-CD44-expressing cells compared with low-CD44-expressing cells (Supplementary Table S1, available at *Carcinogenesis* Online). We also selected all 41 miRNAs that were raised as candidates for directly targeting the human CD44 3′-UTR by using online databases (miRTarBase, TarBase, microRNA.org and TargetScanHuman). We then selected three miRNAs (miR-328, miR-373 and miR-520c) that met both these requirements (Figure 1B). Previous studies characterized miR-520c and miR-373, belonging to the miR-520/373 family, as oncogenes implicated in cancer cell migration and invasion, but with no effect on cancer cell proliferation (21).

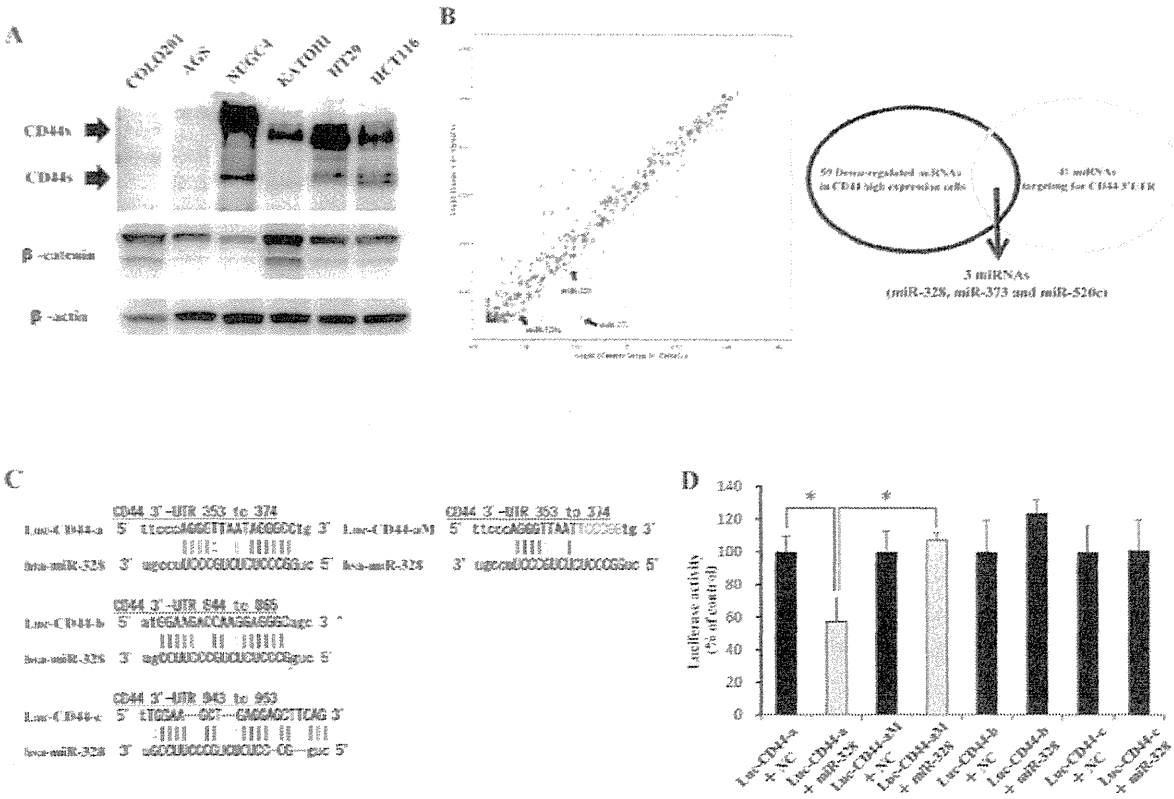

Fig. 1. *Identification of miR-328 directly regulating CD44 expression in gastrointestinal cancer cells.* (A) Immunoblot analysis of CD44, β-catenin and β-actin (loading control) in indicated gastrointestinal cancer cell lines. (B) The left panel shows scatter plots of miRNA expression in high-CD44-expressing cells compared with low-CD44-expressing cells. The right panel shows schematic representation of three miRNAs that met the requirements for regulating CD44 expression. (C) Alignment of the three predicted miR-328 target sequences in the 3′-UTR and the mutated sequence of miR-328-targeting 3′-UTR of CD44 mRNA. The seed match sequences for miR-328 are indicated by lines. (D) Luciferase activity of HCT116 cells transfected with constructed plasmids containing wild-type or mutant miR-328 target sequences in the 3′-UTR of CD44 mRNA and co-transfected with mimic control or mimic miR-328, respectively (*$P < 0.03$).

miR-328, however, was recently shown to be downregulated in colorectal cancer and to regulate CSC-like side-population cells by targeting adenosine triphosphate-binding cassette subfamily G member 2 and matrix metalloproteinase 16 (22). Because CD44 is overexpressed and implicated in the proliferation of cancer cells, we therefore focused on miR-328 for further analysis.

CD44 is a direct target of miR-328

We investigated if miR-328 directly targeted the 3′-UTR of CD44 using constructs containing the putative miR-328 target site or a mutated sequence of the 3′-UTR of CD44 cloned immediately downstream of the luciferase reporter gene. We checked the predicted target sequence of miR-328 in the CD44 3′-UTR using miRanda algorithm. LUC-CD44-a, -b and -c represent alignments of the predicted miR-328 target sequences in the CD44 3′-UTR mRNA. Seed sequences are indicated by lines in Figure 1C. HCT116 cells transfected with a miR-328 mimic significantly suppressed luciferase activity from the reporter vectors containing the wild-type CD44 3′-UTR, LUC-CD44-a, but not LUC-CD44-b and -c, compared with the control vectors (Figure 1D). We also constructed reporter vectors containing the mutated CD44 3′-UTR, LUC-CD44-aM (Figure 1C). HCT116 cells transfected with a miR-328 mimic did not suppress luciferase activity from the reporter vectors containing the mutated 3′-UTR of CD44, LUC-CD44-aM, compared with the wild-type 3′-UTR-containing vector (Figure 1D). These results indicate that miR-328 regulated CD44 expression by directly targeting its 3′-UTR, 353–374.

CD44 expression is correlated with miR-328 expression in patients with gastric cancer

We analyzed the levels of miR-328 expression in gastric cancer tissues and normal gastric epithelium using qRT–PCR. miR-328 expression was significantly suppressed in cancer tissues compared with normal gastric epithelium (Figure 2A). Furthermore, we compared miR-328 expression levels between high- and low-CD44v9-expressing gastric cancer tissues. High CD44v9 expression levels were identified in gastric cancer cells in 62% (39/63) of samples. Interestingly, high CD44v9 expression was significantly associated with low miR-328 expression, whereas low CD44v9 expression was significantly associated with high miR-328 expression (Figure 2B).

miR-328 expression affects cancer cell growth and drug resistance through changes in CD44 expression

To examine the functional relevance of miR-328 expression, we analyzed its expression levels in high-CD44-expressing cancer cell lines (KATOIII and HCT116) transfected with miR-328 mimics, using RT–PCR. miR-328 expression was significantly increased in KATOIII and HCT116 cells transfected with mimic miR-328 compared with controls (Supplementary Figure S1A and B, available at *Carcinogenesis* Online). Western blotting analysis revealed that CD44 protein levels, regardless of β-catenin expression, were significantly reduced in KATOIII and HCT116 cells transfected with miR-328 mimics compared with controls (Figure 3A and C). However, the fact that CD44 mRNA levels were not significantly reduced in HCT116 cells transfected with miR-328 mimics compared with controls, as indicated by qRT–PCR analysis, suggests that miR-328 have some effect on CD44 mRNA and strongly reduces CD44 protein level. (Supplementary Figure S1C, available at *Carcinogenesis* Online). According to our and others' observations, CD44 is known to be overexpressed in cancer cell lines, as well as in primary tissues, and to regulate the proliferative capacity of a variety of tumor types (8,20,23). We, therefore, hypothesized that overexpression of miR-328 in gastrointestinal cancer cells might affect cell proliferation through CD44 downregulation. We, therefore, performed proliferation assays and determined that cell growth was significantly reduced in KATOIII and HCT116 cells transfected with miR-328 mimics compared with controls (Figure 3B and D). We subsequently knocked down miR-328 in low-CD44-expressing AGS cancer cells by transfection with miR-328 inhibitor and performed cell

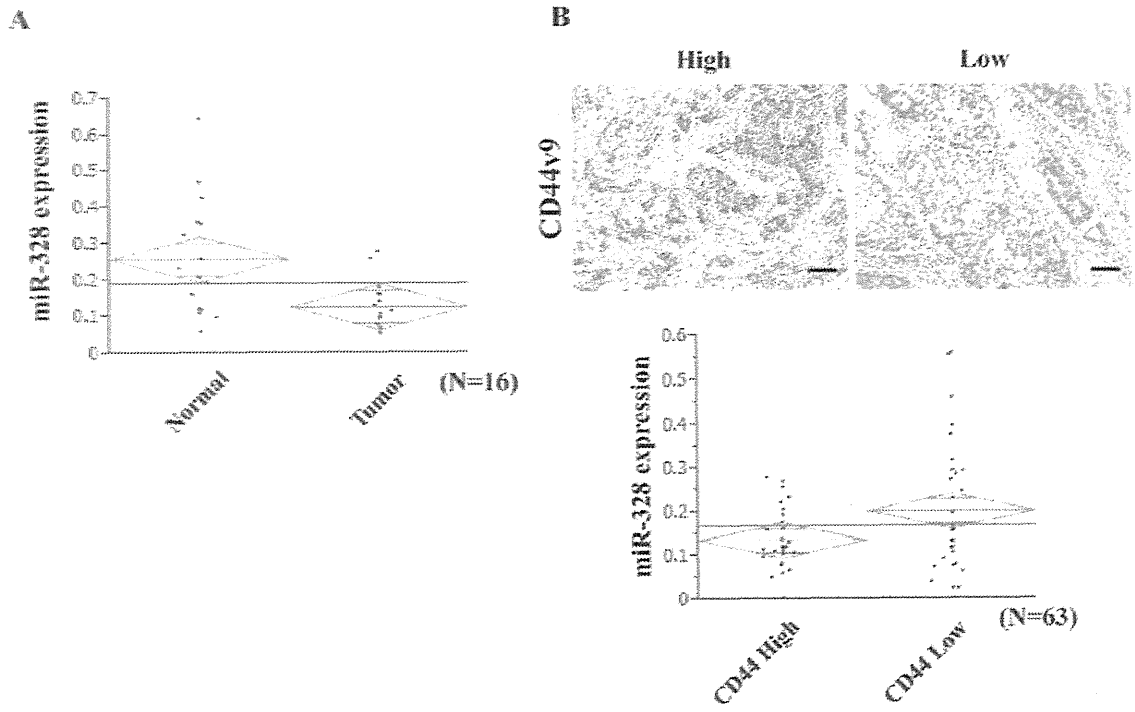

Fig. 2. miR-328 and CD44v9 expression in human gastric mucosa and cancer tissues. (A) Expression of miR-328 in paired normal gastric mucosa and gastric cancer tissues. There was a significant difference in miR-328 expression between these two groups ($P < 0.01$). (B) Upper images show CD44v9 expression pattern in gastric cancer. Lower panel shows expression of miR-328 in high- and low-CD44v9-expressing gastric cancers. Scale bars, 100 μm. There was a significant difference in miR-328 expression between these two groups ($P < 0.01$).

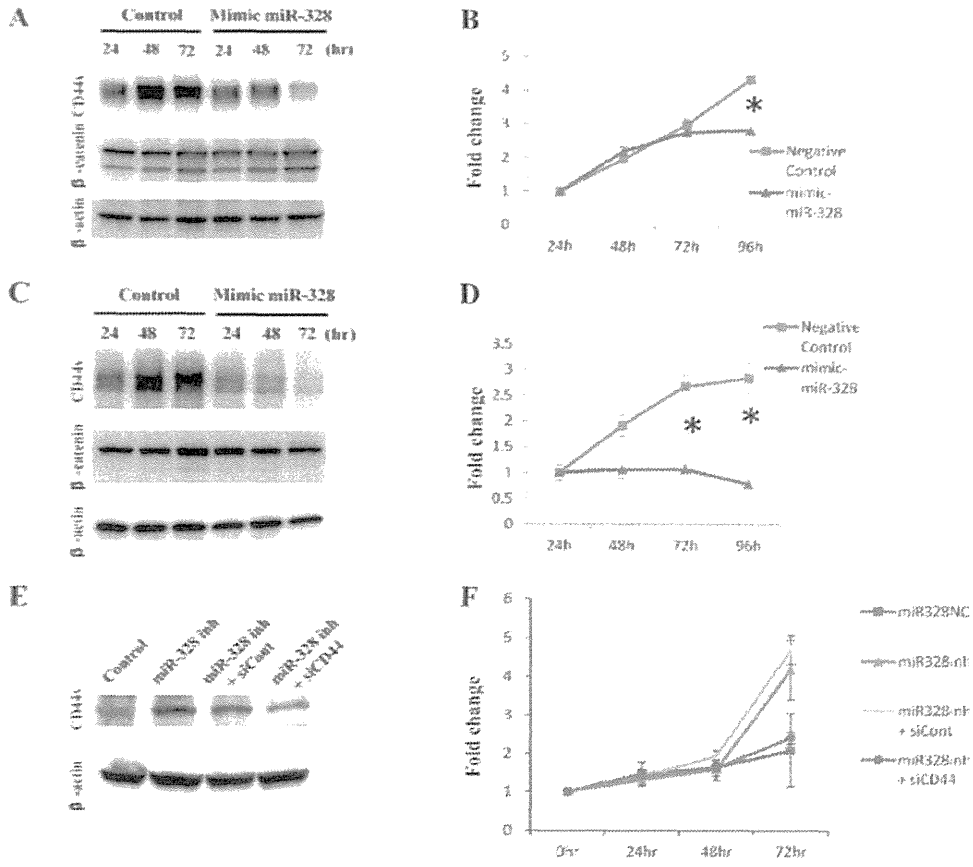

Fig. 3. miR-328 suppresses CD44 expression and cancer cell growth. (A) Immunoblot analysis of CD44 and β-catenin in KATOIII cells transfected with control or mimic miR-328 for the indicated times. β-Actin was similarly analyzed as a loading control. (B) Growth assay analysis in KATOIII cells transfected with control or mimic miR-328. Data are given as means ± SD from triplicate experiments (*$P < 0.01$). (C) Immunoblot analysis of CD44 and β-catenin in HCT116 cells transfected with control or mimic miR-328 for the indicated times. β-Actin was similarly analyzed as a loading control. (D) Growth assay analysis in HCT116 cells transfected with control or mimic miR-328. Data are given as means ± SD from triplicate experiments (*$P < 0.01$). (E) Immunoblot analysis of CD44 expression in AGS cells transfected with control, miR-328 inhibitor, miR-328 inhibitor + control siRNA and miR-328 inhibitor + CD44 siRNA. β-Actin was used as a loading control. (F) Growth assay analysis in AGS cells transfected with control, miR-328 inhibitor, miR-328 inhibitor + control siRNA and miR-328 inhibitor + CD44 siRNA.

proliferation assays. AGS cells transfected with miR-328 inhibitor showed significantly increased CD44 expression and cell growth. Furthermore, AGS cells co-transfected with miR-328 inhibitor and CD44 siRNA showed significantly reduced CD44 expression and cell growth (Figure 3E and F). Given our previous observation that CD44v expression was implicated in resistance to H_2O_2 and to ROS-inducing anticancer drugs such as CDDP (8), we further investigated the viability of HCT116 cells transfected with miR-328 mimics and exposed to H_2O_2 or CDDP. HCT116 cells transfected with miR-328 mimics were significantly less resistant to H_2O_2 and CDDP than control HCT116 cells (Figure 4A). We performed further experiments with the CD44v8-10 expression construct. HCT116 cells co-transfected with mimic miR-328 and CD44v8-10 vector were significantly more resistant to H_2O_2 and CDDP than cells co-transfected with mimic miR-328 and mock vector (Figure 4B and Supplementary Figure S2A, available at *Carcinogenesis* Online). To determine if miR-328 expression affected tumor cell expansion *in vivo*, we prepared miR-328 stably expressing HCT116 cells and examined their tumorigenicity *in vivo*. HCT116 cells stably expressing miR-328 showed significantly reduced CD44 expression and formed significantly smaller tumors in nude mice than cells expressing a mock vector (Figure 4C and D and Supplementary Figure S2B, available at *Carcinogenesis* Online). These results suggest that miR-328 plays a role in regulating CD44 expression to suppress the growth of gastrointestinal cancer cells, and reduce their antioxidative capacity and resistance to chemotherapeutic drugs.

Oxidative stress by M1- and M2-polarized THP-1 macrophages induced downregulation of miR-328 and upregulation of CD44

Tumor necrosis factor (TNF) is a major inducer of chronic inflammation and ROS and is abundant under conditions of chronic inflammation, whereas CD44 expression is induced by these stimuli at inflammatory sites (16,24). We, therefore, examined CD44 expression levels and showed that CD44 expression in AGS cells was increased by TNFα treatment or H_2O_2 treatment in a concentration-dependent manner (Figure 5A). Further, miR-328 expression was markedly suppressed in AGS cells treated with H_2O_2, but not TNFα (Figure 5B). To assess the contribution of oxidative stress to miR-328 expression further, we revealed that H_2O_2-induced miR-328 downregulation was significantly inhibited by treatment with *N*-acetylcysteine (NAC), a powerful antioxidant (Figure 5C). These results suggested that CD44 upregulation in gastric cancer cells may be enhanced through miR-328 downregulation by oxidative stress in the tumor microenvironment. Macrophages are known to produce ROS during phagocytosis and in response to various stimuli, and macrophage-generated oxidants may act as carcinogens causing both tumor initiation and promotion (25). Thus, we investigated if macrophage-derived ROS affected the expression of miR-328 and CD44

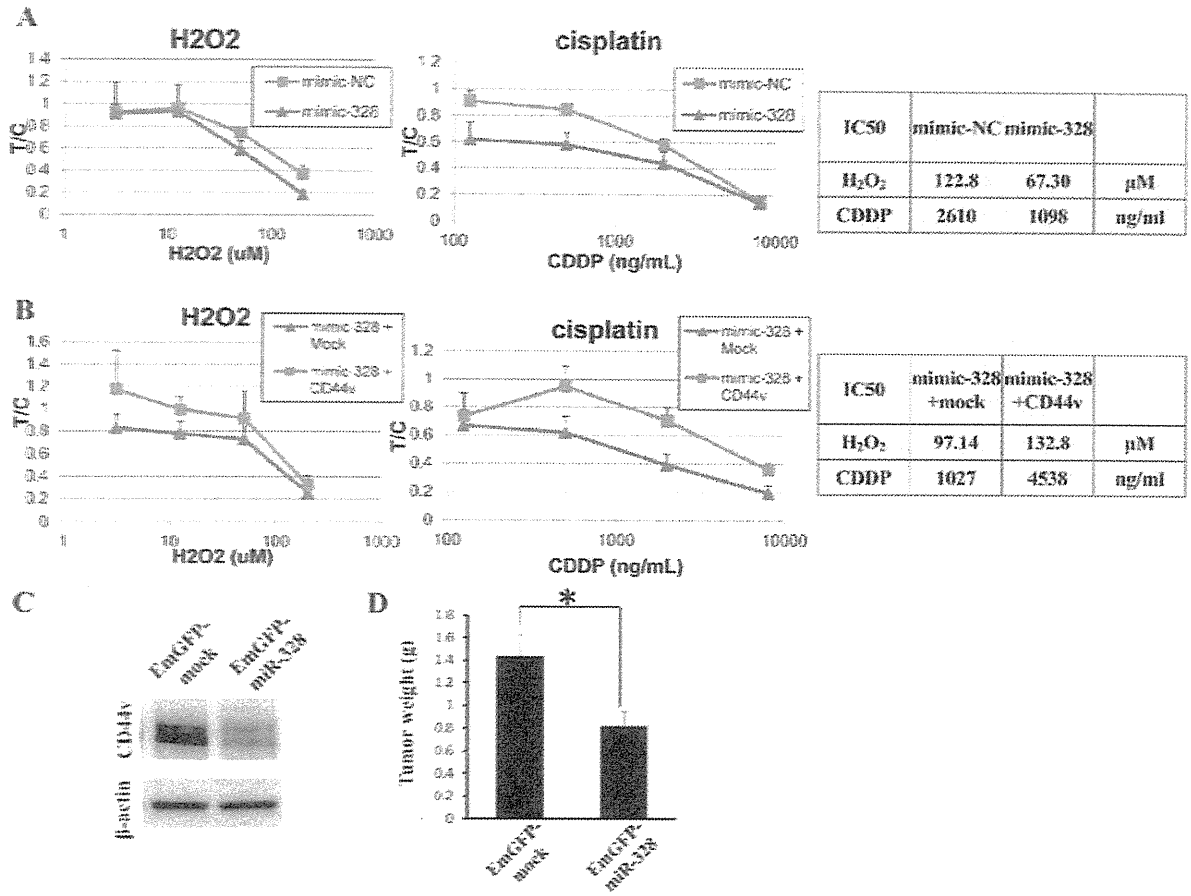

Fig. 4. miR-328 decreases resistance to ROS and chemotherapeutic drug and suppresses cancer cell growth *in vivo*. (**A**) HCT116 cells transfected with control or mimic miR-328 were incubated for 72 h with the indicated concentrations of H_2O_2 or CDDP and then assayed for cell viability. Data are expressed as treated/control cell ratio and are mean ± SD from triplicate experiments. The median inhibitory concentration (IC_{50}) values are also shown. (**B**) HCT116 cells co-transfected with mimic miR-328 + mock vector or mimic miR-328 + CD44v8-10 were incubated for 72 h with the indicated concentrations of H_2O_2 or CDDP and assayed for cell viability. Data are expressed as treated/control cell ratio and are given as mean ± SD from triplicate experiments. The median inhibitory concentration (IC_{50}) values are also shown. (**C**) Immunoblot analysis of CD44 in HCT116 cells stably transfected with mock or miR-328 vector. (**D**) Weights of tumors formed by HCT116 cells stably transfected with control or miR-328 vector were determined at 35 days after cell injection. Data are given as mean ± SD for five animals in each group. $^*P < 0.01$.

in gastrointestinal cancer cells. We co-cultured M1- and M2-polarized THP-1 macrophages with low-CD44-expressing AGS gastric cancer cells (Supplementary Figure S3A, available at *Carcinogenesis* Online) (26). Consistent with previous research, M1- and M2-polarized THP-1 macrophages showed a distinct cytokine-production profile (e.g. IL-12, IL-1β, TNFα, IL-6; Supplementary Figure S3B, available at *Carcinogenesis* Online). M1- and M2-polarized THP-1 macrophages were then co-cultured with AGS cells for 24 h and examined by fluorescence microscopy after staining with the ROS-sensitive fluorescent probe 2′,7′-dichlorofluorescein diacetate. M1- and M2-polarized macrophages showed abundant ROS and pronounced 2′,7′-dichlorofluorescein diacetate staining (Supplementary Figure S3C, available at *Carcinogenesis* Online). qRT–PCR analysis revealed that miR-328 expression was significantly decreased and CD44 expression was conversely increased in AGS cells co-cultured with both M1- and M2-polarized THP-1 macrophages, and these changes were notably recovered by NAC treatment (Figure 5D and E). Flow cytometry further demonstrated that CD44 protein expression was significantly increased by miR-328 suppression in AGS cells in both M1- and M2-conditioned medium, compared with controls (Figure 5F). To investigate the effects of macrophages on cell growth, we performed proliferation assays using M1 and M2 macrophage-conditioned medium and determined that cell growth was significantly increased in AGS cells in either M1- or M2-conditioned medium, compared with controls (Figure 5G). Together, these results suggest that macrophage-derived ROS are involved in CD44 upregulation and cell growth through miR-328 downregulation.

Increased infiltrated macrophages in tumor stroma correlated with CD44 upregulation and miR-328 downregulation in gastric cancer cells

We, therefore, investigated if the macrophage-infiltration rate correlated with CD44 and miR-328 expression in gastric cancer tissues. We examined the expression of CD44v9 and the macrophage markers CD68 and CD163 by IHC analysis, and miR-328 expression by qRT–PCR in samples from 63 patients with gastric cancer. Pan-macrophages were detected by immunostaining of CD68, and the M2 population was evaluated by immunostaining of CD163, as described previously (18). Infiltration of CD68+ macrophages correlated with high CD44v9 expression and low miR-328 expression in gastric cancer cells (Figure 6A and B), whereas infiltration of CD163+ macrophages correlated with high CD44v9 expression and low miR-328 expression (Figure 6C and D). These results suggest that the number of infiltrated macrophage in the tumor stroma was significantly associated with CD44 upregulation and miR-328 downregulation in patients with gastric cancer.

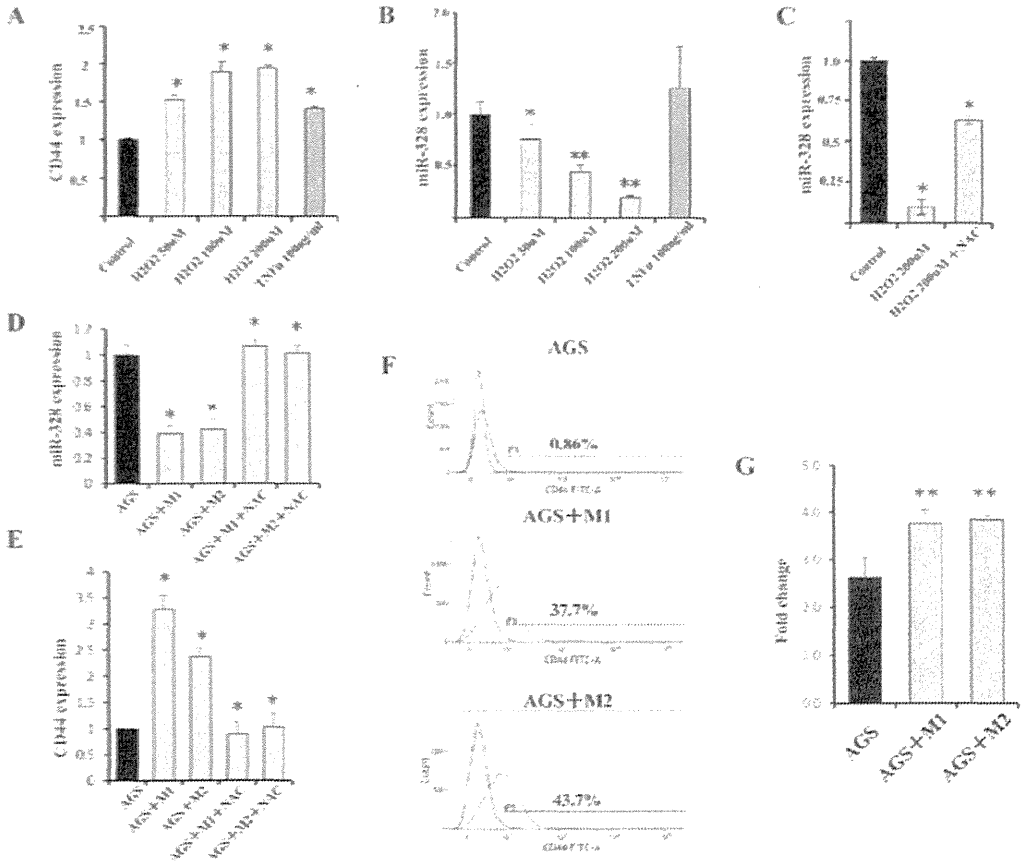

Fig. 5. Oxidative stress produced by macrophages induces miR-328 downregulation and CD44 upregulation in AGS cells. (A) qRT–PCR analysis of CD44 mRNA in AGS cells treated with H_2O_2 or TNFα at the indicated concentrations. Data were normalized by the amount of glyceraldehyde-3-phosphate dehydrogenase mRNA and are given as means ± SD from triplicate experiments ($^*P < 0.01$). (B) qRT–PCR analysis of miR-328 in AGS cells treated with H_2O_2 or TNFα at the indicated concentrations. Data were normalized by the amount of RNU6B and are given as means ± SD from triplicate experiments ($^*P < 0.03$, $^{**}P < 0.01$). (C) qRT–PCR analysis of miR-328 in AGS cells treated with 200 μM H_2O_2 in the absence or presence of 5 mM NAC. Data were normalized by the amount of RNU6B and are given as means ± SD from triplicate experiments ($^*P < 0.01$). (D) qRT–PCR analysis of miR-328 in AGS cells co-cultured with M1- or M2-polarized macrophages in the absence or presence of 5 mM NAC, compared with AGS cells without co-culture. Data were normalized by the amount of RNU6B and are given as means ± SD from triplicate experiments ($^*P < 0.01$). (E) qRT–PCR analysis of CD44 in AGS cells co-cultured with M1- or M2-polarized macrophage in the absence or presence of 5 mM NAC, compared with AGS cells without co-culture. Data were normalized by the amount of glyceraldehyde-3-phosphate dehydrogenase mRNA and are given as means ± SD from triplicate experiments ($^*P < 0.01$). (F) Flow cytometric analysis of CD44 in AGS cells in normal medium, or M1- or M2-polarized macrophage-conditioned medium. (G) Growth assay analysis in AGS cells in normal medium, or M1- or M2-polarized macrophage-conditioned medium for 48 h.

Discussion

We previously reported that CD44 is not only a major CSC marker but also plays a functional role in ROS defense, resulting in tumor development and colonization of metastatic cancer cells (8,27). Persistent ROS stress may induce adaptive stress responses, including the upregulation of redox-sensitive transcription factors, antioxidants and survival factors. Redox adaptation not only enables cancer cells to survive under increased ROS stress but also renders them resistant to certain anticancer drugs (28,29). CD44-related signaling thus provides a potential therapeutic target, but the mechanisms regulating CD44 expression in cancer cells remain incompletely understood. Several miRNAs suppress CD44 expression by targeting the CD44 3′-UTR, resulting in suppression of tumorigenesis and metastasis. For instance, miR-34a is a key negative regulator of CD44+ prostate CSCs and inhibits metastasis by directly repressing CD44, whereas miR-199a targets CD44 to suppress tumorigenicity and multidrug resistance in CD44+/CD117+ ovarian cancer-initiating cells (30,31). Based on these previous studies, we speculated that miRNAs may be a key factor in CD44 upregulation in gastrointestinal cancer cells. We, therefore, performed miRNA screening and identified the candidate miRNA, miR-328, in gastrointestinal cancer cell lines. The results of this study demonstrated that miR-328 modulated CD44 expression by directly targeting the CD44 3′-UTR and identified the miR-328-targeting sequences within the CD44 3′-UTR. A previous study demonstrated that miR-328 regulated zonation morphogenesis by targeting CD44 expression (32). We examined three candidate miR-328 binding sites (353–374, 844–865 and 943–965) in the CD44 3′-UTR using the miRanda algorithm and identified the miR-328 target sequence (353–374). This study provides the first characterization of this target sequence. Furthermore, we clarified that miR-328 expression affected cancer cell growth and chemotherapeutic drug and ROS resistance. CD44 expression in gastric cancer cells was triggered by ROS and inflammatory cytokines, and oxidative stress by H_2O_2 suppressed miR-328 expression in a concentration-dependent manner. However, TNFα had no effect on miR-328 expression in gastric cancer cells. Thus, although this study provides evidence that miR-328 expression is modulated by oxidative stress, the precise mechanism of miR-328 regulation remains unknown. Previous studies have shown that miRNA expression can be deregulated by epigenetic alterations, including aberrant DNA methylation, and such mechanisms may be implicated in the regulation of miR-328 by oxidative stress (33,34).

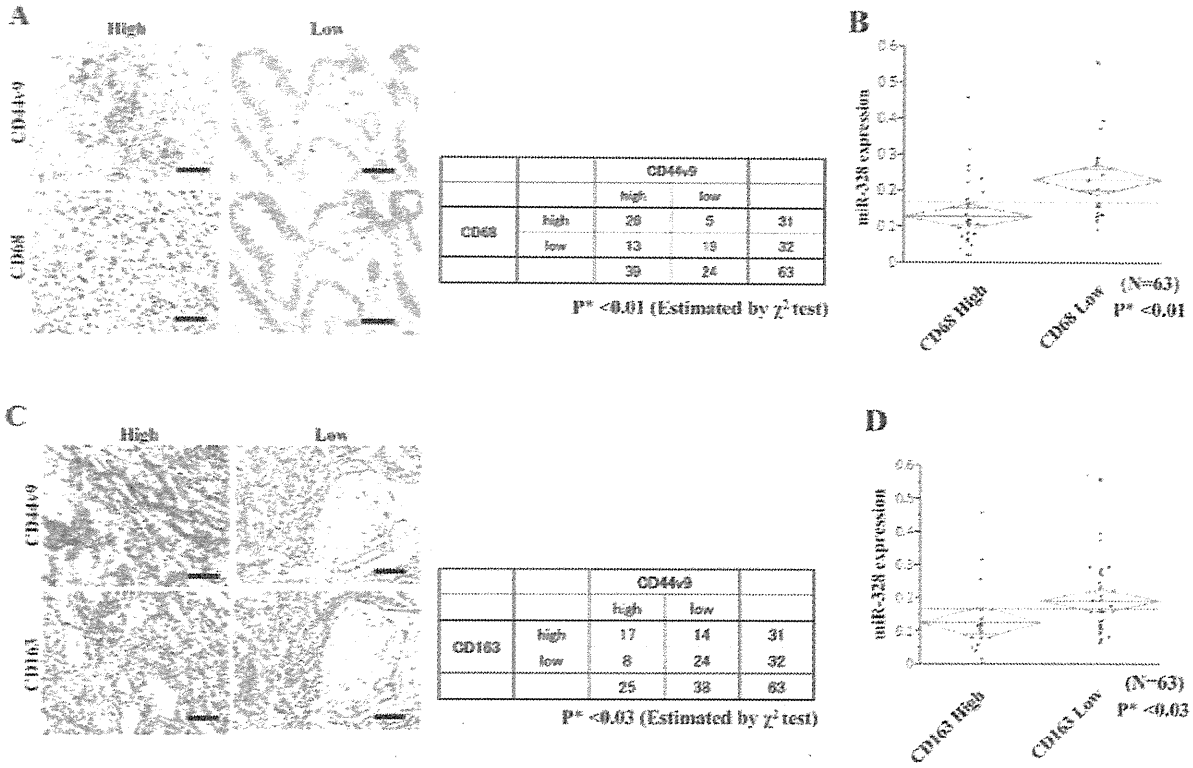

Fig. 6. Correlations between the numbers of CD68+ and CD163+ macrophages and upregulation of CD44 expression and downregulation of miR-328 in human gastric cancer. (**A**) Left images show CD44v9 and CD68 expression patterns in gastric cancer. Scale bars, 100 μm. Right panel shows the correlation between CD44v9 expression status in gastric cancer cells and CD68-expressing macrophages in gastric cancer stroma. There was a significant correlation between these two groups (*$P < 0.01$). (**B**) Expression of miR-328 in gastric stroma tissues with high and low levels of CD68 macrophages. There was a significant difference in miR-328 expression between these two groups (*$P < 0.01$). (**C**) Left images show CD44v9 and CD163 expression patterns in gastric cancer. Scale bars, 100 μm. Right panel shows correlation between CD44v9 expression status in gastric cancer cells and CD163-expressing macrophages in gastric cancer stroma. There was a significant correlation between these two groups (*$P < 0.03$). (**D**) Expression of miR-328 in gastric stroma tissues with high and low levels of CD163 macrophages. There was a significant difference in miR-328 expression between these two groups (*$P < 0.03$).

Therefore, further investigations are needed to reveal the mechanism of miR-328 suppression by oxidative stress.

In cancer tissues, ROS is produced by a variety of cell types, including neutrophils, macrophages and endothelial cells. We recently showed that ablation of CD44 in the Gan mouse genetic gastric cancer model, triggered tumor-cell growth arrest through ROS-mediated signals, resulting in tumor suppression. Abundant macrophages infiltrated into the tumor stroma in Gan mouse tumors, and these macrophages have been reported to contribute to CD44 expression and gastric tumor progression through inflammatory cytokines (35,36). In this study, we revealed that infiltrated macrophages in the tumor microenvironment may contribute to redox adaptation through CD44 upregulation by miR-328 suppression. Previous studies have shown that M2 macrophages are associated with a poorer prognosis in various types of cancer (18,37,38); however, M2 macrophages are correlated with a good prognosis in gastrointestinal cancer (39,40), suggesting that the different functional roles of M1- and M2-polarized macrophages depend on the state of the cancer cells and the organ. Furthermore, recent studies have provided evidence indicating functional plasticity of M1/M2 macrophages in response to different microenvironmental signals (41,42). The present results indicated that both of M1- and M2-polarized macrophages triggered CD44 expression through miR-328 suppression, suggesting no difference between these two types of macrophages in terms of miR-328 suppression and CD44 induction. The number of infiltrated macrophages was also significantly associated with CD44 upregulation and miR-328 downregulation in gastric cancer patients. These findings reveal that infiltrated macrophages in the tumor microenvironment cause CD44 upregulation through miR-328 suppression. CD44 is implicated in redox adaptation, resulting in cancer cell growth and resistance to chemotherapeutic drugs through enhanced ROS defense.

In conclusion, the results of this study reveal a new redox adaptation mechanism in gastrointestinal cancer and indicate that miR-328-CD44 signaling mediated by macrophages may represent a novel therapeutic target for gastrointestinal cancer treatment.

Supplementary material

Supplementary Tables S1, S2 and Figures S1–S3 can be found at http://carcin.oxfordjournals.org/

Funding

Okukubo Memorial Fund for Medical Research at Kumamoto University School of Medicine; Medical Research Encouragement Prize of the Japan Medical Association; Japan Society for the Promotion of Science grant-in-aid for scientific research (24591912).

Conflict of Interest Statement: None declared.

References

1. Al-Hajj,M. *et al.* (2003) Prospective identification of tumorigenic breast cancer cells. *Proc. Natl Acad. Sci. USA*, **100**, 3983–3988.
2. Collins,A.T. *et al.* (2005) Prospective identification of tumorigenic prostate cancer stem cells. *Cancer Res.*, **65**, 10946–10951.

3. Dalerba,P. *et al.* (2007) Phenotypic characterization of human colorectal cancer stem cells. *Proc. Natl Acad. Sci. USA.*, **104**, 10158–10163.
4. Ponta,H. *et al.* (2003) CD44: from adhesion molecules to signalling regulators. *Nat. Rev. Mol. Cell Biol.*, **4**, 33–45.
5. Nagano,O. *et al.* (2004) Mechanism and biological significance of CD44 cleavage. *Cancer Sci.*, **95**, 930–935.
6. Tanabe,K.K. *et al.* (1993) Expression of CD44R1 adhesion molecule in colon carcinomas and metastases. *Lancet*, **341**, 725–726.
7. Ishimoto,T. *et al.* (2010) CD44+ slow-cycling tumor cell expansion is triggered by cooperative actions of Wnt and prostaglandin E2 in gastric tumorigenesis. *Cancer Sci.*, **101**, 673–678.
8. Ishimoto,T. *et al.* (2011) CD44 variant regulates redox status in cancer cells by stabilizing the xCT subunit of system xc(-) and thereby promotes tumor growth. *Cancer Cell*, **19**, 387–400.
9. Lewis,B.P. *et al.* (2005) Conserved seed pairing, often flanked by adenosines, indicates that thousands of human genes are microRNA targets. *Cell*, **120**, 15–20.
10. Zhang,B. *et al.* (2007) microRNAs as oncogenes and tumor suppressors. *Dev. Biol.*, **302**, 1–12.
11. Kong,Y.W. *et al.* (2012) microRNAs in cancer management. *Lancet Oncol.*, **13**, e249–e258.
12. Hao,N.B. *et al.* (2012) Macrophages in tumor microenvironments and the progression of tumors. *Clin. Dev. Immunol.*, **2012**, 948098.
13. Martinez,F.O. *et al.* (2006) Transcriptional profiling of the human monocyte-to-macrophage differentiation and polarization: new molecules and patterns of gene expression. *J. Immunol.*, **177**, 7303–7311.
14. De Palma M. *et al.* (2013) Macrophage regulation of tumor responses to anticancer therapies. *Cancer cell*, **23**, 277–286.
15. Sica,A. *et al.* (2012) Macrophage plasticity and polarization: *in vivo* veritas. *J. Clin. Invest.*, **122**, 787–795.
16. Fan,X. *et al.* (1996) Expression of CD44 and its variants on gastric epithelial cells of patients with *Helicobacter pylori* colonisation. *Gut*, **38**, 507–512.
17. Okamoto,I. *et al.* (1999) CD44 cleavage induced by a membrane-associated metalloprotease plays a critical role in tumor cell migration. *Oncogene*, **18**, 1435–1446.
18. Hasita,H. *et al.* (2010) Significance of alternatively activated macrophages in patients with intrahepatic cholangiocarcinoma. *Cancer Sci.*, **101**, 1913–1919.
19. Mima,K. *et al.* (2012) CD44s regulates the TGF-β-mediated mesenchymal phenotype and is associated with poor prognosis in patients with hepatocellular carcinoma. *Cancer Res.*, **72**, 3414–3423.
20. Zeilstra,J. *et al.* (2008) Deletion of the WNT target and cancer stem cell marker CD44 in Apc(Min/+) mice attenuates intestinal tumorigenesis. *Cancer Res.*, **68**, 3655–3661.
21. Huang,Q. *et al.* (2008) The microRNAs miR-373 and miR-520c promote tumour invasion and metastasis. *Nat. Cell Biol.*, **10**, 202–210.
22. Xu,X.T. *et al.* (2012) MicroRNA expression profiling identifies miR-328 regulates cancer stem cell-like SP cells in colorectal cancer. *Br. J. Cancer*, **106**, 1320–1330.
23. Du,L. *et al.* (2008) CD44 is of functional importance for colorectal cancer stem cells. *Clin. Cancer Res.*, **14**, 6751–6760.
24. Hayer,S. *et al.* (2005) CD44 is a determinant of inflammatory bone loss. *J. Exp. Med.*, **201**, 903–914.
25. Weitzman,S.A. *et al.* (1990) Inflammation and cancer: role of phagocyte-generated oxidants in carcinogenesis. *Blood*, **76**, 655–663.
26. Tjiu,J.W. *et al.* (2009) Tumor-associated macrophage-induced invasion and angiogenesis of human basal cell carcinoma cells by cyclooxygenase-2 induction. *J. Invest. Dermatol.*, **129**, 1016–1025.
27. Yae,T. *et al.* (2012) Alternative splicing of CD44 mRNA by ESRP1 enhances lung colonization of metastatic cancer cell. *Nat. Commun.*, **3**, 883.
28. Trachootham,D. *et al.* (2009) Targeting cancer cells by ROS-mediated mechanisms: a radical therapeutic approach? *Nat. Rev. Drug Discov.*, **8**, 579–591.
29. Nagano,O. *et al.* (2013) Redox regulation in stem-like cancer cells by CD44 variant isoforms. *Oncogene*, **32**, 5191–5198.
30. Liu,C. *et al.* (2011) The microRNA miR-34a inhibits prostate cancer stem cells and metastasis by directly repressing CD44. *Nat. Med.*, **17**, 211–215.
31. Cheng,W. *et al.* (2012) MicroRNA-199a targets CD44 to suppress the tumorigenicity and multidrug resistance of ovarian cancer-initiating cells. *FEBS J.*, **279**, 2047–2059.
32. Wang,C.H. *et al.* (2008) MicroRNA miR-328 regulates zonation morphogenesis by targeting CD44 expression. *PLoS One*, **3**, e2420.
33. Zhang,S. *et al.* (2011) Downregulation of miR-132 by promoter methylation contributes to pancreatic cancer development. *Carcinogenesis*, **32**, 1183–1189.
34. Baer,C. *et al.* (2013) Genome-wide epigenetic regulation of miRNAs in cancer. *Cancer Res.*, **73**, 473–477.
35. Oguma,K. *et al.* (2008) Activated macrophages promote Wnt signalling through tumour necrosis factor-alpha in gastric tumour cells. *EMBO J.*, **27**, 1671–1681.
36. Oshima,H. *et al.* (2006) Carcinogenesis in mouse stomach by simultaneous activation of the Wnt signaling and prostaglandin E2 pathway. *Gastroenterology*, **131**, 1086–1095.
37. Jensen,T.O. *et al.* (2009) Macrophage markers in serum and tumor have prognostic impact in American Joint Committee on Cancer stage I/II melanoma. *J. Clin. Oncol.*, **27**, 3330–3337.
38. Komohara,Y. *et al.* (2008) Possible involvement of the M2 anti-inflammatory macrophage phenotype in growth of human gliomas. *J. Pathol.*, **216**, 15–24.
39. Leung,S.Y. *et al.* (2004) Expression profiling identifies chemokine (C-C motif) ligand 18 as an independent prognostic indicator in gastric cancer. *Gastroenterology*, **127**, 457–469.
40. Nagorsen,D. *et al.* (2007) Tumor-infiltrating macrophages and dendritic cells in human colorectal cancer: relation to local regulatory T cells, systemic T-cell response against tumor-associated antigens and survival. *J. Transl. Med.*, **5**, 62.
41. Saccani,A. *et al.* (2006) p50 nuclear factor-kappaB overexpression in tumor-associated macrophages inhibits M1 inflammatory responses and antitumor resistance. *Cancer Res.*, **66**, 11432–11440.
42. Guiducci,C. *et al.* (2005) Redirecting *in vivo* elicited tumor infiltrating macrophages and dendritic cells towards tumor rejection. *Cancer Res.*, **65**, 3437–3446.

Received July 2, 2013; revised October 26, 2013; accepted November 27, 2013

IJC
International Journal of Cancer

Expression of TNF-α and CD44 is implicated in poor prognosis, cancer cell invasion, metastasis and resistance to the sunitinib treatment in clear cell renal cell carcinomas

Shuji Mikami[1], Ryuichi Mizuno[2], Takeo Kosaka[2], Hideyuki Saya[3], Mototsugu Oya[2] and Yasunori Okada[4]

[1] Division of Diagnostic Pathology, Keio University Hospital, School of Medicine, Keio University, Tokyo, Japan
[2] Department of Urology, School of Medicine, Keio University, Tokyo, Japan
[3] Division of Gene Regulation, Institute for Advanced Medical Research, School of Medicine, Keio University, Tokyo, Japan
[4] Department of Pathology, School of Medicine, Keio University, Tokyo, Japan

Tumor necrosis factor-α (TNF-α) is involved in epithelial-mesenchymal transition (EMT) and expression of CD44, a cancer stem cell marker, in several cancers. This study was performed to clarify the significance of TNF-α and CD44 in clear cell renal cell carcinomas (ccRCCs). Expression of TNF-α and CD44 was examined by immunohistochemistry in 120 ccRCCs. Involvement of TNF-α in EMT and induction of CD44 was analyzed by monitoring expression of EMT-related genes and CD44, and invasion in cultured ccRCC cell lines. TNF-α and CD44 were immunolocalized mainly to carcinoma cells of high-grade ccRCCs with positive correlations with primary tumor stage. A positive correlation was also obtained between TNF-α and CD44 expression, and co-upregulation of TNF-α and CD44 was associated with primary tumor stage, distant metastasis, and poor prognosis. TNF-α enhanced migration and invasion of ccRCC cells together with down-regulation of E-cadherin expression and up-regulation of matrix metalloproteinase 9 and CD44 expression. TNF-α also up-regulated the expression of TNF-α itself in ccRCC cells. Among the 25 ccRCC patients treated with sunitinib for metastatic disease, high CD44 expression was associated with poor treatment outcome. Importantly, residual carcinoma cells in the sunitinib-treated metastatic ccRCCs were strongly positive for CD44, and the CD44 expression was significantly higher in the tumors from the sunitinib-treated patients than in those from untreated ones. Our data show that TNF-α plays an important role in progression of ccRCCs by inducing EMT and CD44 expression, and suggest that CD44 induced by TNF-α may be involved in the resistance to the sunitinib treatment.

Cancer-related inflammation accelerates tumor cell proliferation and angiogenesis.[1] Tumor necrosis factor-α (TNF-α) is an important mediator for the inflammatory responses in cancers, and infiltrated macrophages are a major source of TNF-α.[2] Although TNF-α was originally reported as a cytokine to induce apoptotic cell death and cachexia,[1] accumulated lines of evidence indicate that TNF-α has tumor-promoting effects.[2] Actually, TNF-α produced by tumor cells is known to induce tumor cell proliferation and progression by autocrine and paracrine manners in ovarian cancers,[3] and TNF-α enhances epithelial-mesenchymal transition (EMT) of clear cell renal cell carcinoma (ccRCC) cells *in vitro*.[4] TNF-α

Key words: TNF-α, epithelial-mesenchymal transition, renal cell carcinoma, MMP, CD44

Abbreviations: ccRCC: clear cell renal cell carcinoma; EMT: epithelial and mesenchymal transition; HE: hematoxylin and eosin; MMP: matrix metalloproteinase; PDGF: platelet-derived growth factor; PET: polyethylene terephthalate; TNF-α, tumor necrosis factor-α; TNM: tumor-node-metastases; VEGF: vascular endothelial growth factor

Additional Supporting Information may be found in the online version of this article.

M.O. has received honoraria and research funding from Pfizer, and other authors declare no conflict of interest

Grant sponsor: Grant-in-Aid for Scientific Research (C); **Grant number:** 25460422; **Grant sponsor:** Grain-in-Aid for Scientific Research (S); **Grant number:** 26221005; **Grant sponsor:** Ministry of Education, Culture, Sports, Science, and Technology of Japan (MEXT) (to S.M.); **Grant sponsor:** Grain-in-Aid for Scientific Research (B); **Grant number:** 24390374 from MEXT (to M.O.); **Grant sponsors:** Project for Development of Innovative Research on Cancer Therapeutics (P-Direct) (to S. M., R.M, K.T. and M.O.) and Grant-in-Aid for Scientific Research (A) from MEXT; **Grant number:** 24249022 (to Y.O.); **Grant sponsor:** Third Term 10-year Strategy for Cancer Control from the Ministry of Health and Welfare (to Y.O.)

DOI: 10.1002/ijc.29137

History: Received 8 Dec 2013; Accepted 23 Jul 2014; Online 14 Aug 2014

Correspondence to: Shuji Mikami, Division of Diagnostic Pathology, Keio University Hospital, 35 Shinanomachi, Shinjuku-ku, Tokyo, 160-8582, Japan, Tel.: +81-3-5363-3844, Fax: +81-3-5363-3644, E-mail: mikami@a7.keio.jp or Yasunori Okada, Department of Pathology, School of Medicine, Keio University, 35 Shinanomachi, Shinjuku-ku, Tokyo, 160-8582, Japan, Tel: +81-3-5363-3763, Fax: +83-3-3353-3290, E-mail: okada@z6.keio.jp